Meteoritics & Planetary Science 31, 749–766 (1996)

An experimental and theoretical study of rare-earth-element partitioning between sulfides (FeS, CaS) and silicate and applications to enstatite achondrites

K. LODDERS

Planetary Chemistry Laboratory, Department of Earth and Planetary Sciences, Washington University, One Brookings Drive, Campus Box 1169, St. Louis, Missouri 63130-4899, USA
Author's e-mail address: klodders@cosmos.win.net.

(Received 1995 May 18; accepted in revised form 1996 June 26)

Abstract–Partition coefficients of the rare-earth-elements (REE) between sulfides (FeS or CaS) and silicate melt were determined experimentally at 1200–1300 °C. The REE sulfide/silicate partition coefficients (D) are ≤1 under the experimental O and S fugacities, which demonstrates that the REE are mainly located in the silicate phase. Rare-earth-element partition coefficients in the FeS/silicate system decrease from light to heavy REE, while the opposite behavior is found for the CaS/silicate system, where partition coefficients increase from light to heavy REE. In both sulfide systems, Eu is preferentially incorporated into the sulfide phases, as also expected from thermodynamic calculations. The Eu sulfide/silicate partition coefficient is about a factor of ten higher than that of neighboring Sm and Gd, in accordance with thermodynamic predictions of REE sulfide/silicate partition coefficients. The low sulfide/silicate partition coefficients indicate that CaS (oldhamite) in enstatite achondrites (aubrites) cannot have gained its high REE concentrations during igneous differentiation processes. The high REE concentrations and the REE patterns in aubritic oldhamite are more plausibly explained by REE condensation into refractory CaS. The refractory nature of CaS prevented major exchange reactions of the oldhamite with other aubritic minerals during the short differentiation and metamorphism period on the aubrite parent body. Thus, oldhamite in aubrites may be relict condensates altered to different degrees during short heating events, as originally suggested by Lodders and Palme (1990).

INTRODUCTION

The distribution of the REE among minerals in differentiated meteorites provides a tool to decipher the differentiation process which led to the formation of these meteorites. In order to apply this tool to the highly reduced and differentiated enstatite achondrites (aubrites), the REE distribution in aubritic minerals and the partition coefficients for the relevant mineral/melt systems need to be known. Several measurements of REE abundances in bulk aubrites and in their individual mineral phases are available (*e.g.*, Schmitt *et al.*, 1963; Masuda, 1967; Wolf *et al.*, 1983; Graham and Henderson, 1985; Floss and Crozaz, 1993; Lodders *et al.*, 1993; Wheelock *et al.*, 1994). Likewise, the REE mineral/melt partition coefficients are known for some common minerals (*e.g.*, pyroxene, olivine, diopside, plagioclase) found in aubrites (Kennedy *et al.*, 1993; Grutzeck *et al.*, 1974; Drake and Weill, 1975). However, oldhamite (ideal formula, CaS) is the main REE carrier in enstatite meteorites (*e.g.*, Larimer and Ganapathy, 1987; Floss *et al.*, 1990; Lodders and Palme, 1991; Kurat *et al.*, 1992; Lundberg and Crozaz, 1995), and CaS/silicate partition coefficients are also necessary for modeling the petrogenesis of aubrites.

Several bulk aubrite samples show relative Eu-depletions when normalized to chondrites (*e.g.*, Wolf *et al.*, 1983), and because Eu and the other REE show chalcophile behavior in aubrites, it is possible that some Eu was removed by a Fe-FeS melt during the formation of the metal-sulfide core (Lodders and Palme, 1989, 1990). Thus, it is necessary to include the REE sulfide/silicate partition coefficients for CaS and FeS in models of igneous differentiation on the aubrite parent body (APB). Preliminary REE sulfide/silicate partitioning data were determined and reported at meetings by several groups (Jones and Boynton, 1983; Lodders and Palme, 1989, 1990; Lodders *et al.*, 1990; Dickinson *et al.*, 1990a,b,c, 1991). Some results were also discussed by Lodders (1991, 1995, 1996). This paper describes more details of the experimental determination of CaS/silicate and FeS/silicate partition coefficients, the theoretical modeling of the partition coefficients, and the implications for the aubrite parent body.

The experimental data together with other crystal/melt partition coefficients are used to model the REE distributions among minerals in aubrites. It is shown below that the REE distribution among aubritic minerals cannot be ascribed to simple crystallization processes because the measured REE concentrations in oldhamite are much too high to be explained by CaS/silicate partitioning. As originally proposed by Lodders and Palme (1990), other processes such as condensation of the REE into CaS from a highly reduced solar gas and metamorphic redistribution of the REE offer more plausible alternative explanations for the observed REE distributions in aubrites.

EXPERIMENTAL PROCEDURES

Rare-earth-element partitioning was investigated in two sulfide/silicate systems. The first system we describe is the 'FeS'/silicate system. Here and elsewhere in the text, we refer to stoichiometric and nonstoichiometric FeS as 'FeS'. The experimental charges consisted of ~200 mg of a tholeiitic basalt (Vogelsberg area, Germany), 200 mg Fe powder, and 60–150 mg S. The composition of the basalt is given in Table 1. The fine powdered basalt was either mixed with REE-oxides at the ppm level suitable for instrumental neutron activation analyses (INAA) or with a selected set of three REE-oxides at the one percent level for electron microprobe (EMP) analyses. In addition, another set of 'FeS'/silicate experiments was done using an oxide glass similar in composition to the basalt but free of Mn, Cr, and Fe. This set of experiments was done to avoid the ^{56}Mn background radiation that disturbs the measurement of short-lived REE isotopes (*e.g.*, ^{165}Dy). The use of a Fe-free starting silicate also helped to monitor the approach to equilibrium because Fe must diffuse from the sulfide into the silicate. The final concentrations of Fe in this silicate after the experiment were indistinguishable from the Fe concentration in the basaltic melt equilibrated with a Fe-sulfide under otherwise similar conditions.

The second system (CaS/silicate) utilized a starting silicate similar in composition to the silicate portion of enstatite chondrites (Table 2). Appro-

TABLE 1. Composition of starting silicates for REE 'FeS'/silicate partitioning experiments and amounts of REE added for INAA.

	Tholeiitic Basalt (wt%)	Oxide Glass (wt%)	REE Spike (ppm)	
MgO	11.67	11.27	La	250
Al_2O_3	11.69	14.59	Pr	1500
SiO_2	49.59	55.28	Nd	1000
CaO	8.76	11.16	Sm	50
TiO_2	2.37	2.96	Eu	30
FeO	10.22*	0.00	Gd	1500
Na_2O	2.43	2.75	Tb	300
K_2O	1.64	1.90	Dy	50
Total	98.37	99.91	Ho	100
			Yb	300
			Lu	40

*All Fe as FeO.

priate oxides (SiO_2, Al_2O_3, MgO, TiO_2) and carbonates (Na_2CO_3, K_2CO_3) and REE-oxides were mixed together and reacted for 24 h at 1000 °C to release CO_2 and then fused at 1500 °C in glassy C crucibles (Sigradur, Germany) under N_2. The use of glassy C crucibles allows easy recovery of the fused silicate. Three starting silicates were prepared: a REE-free silicate for reversal experiments (series I in Table 2); a silicate containing Sm, Eu, Gd (series II); and a silicate containing La, Yb, and Lu (series III). About one wt% of each REE-oxide was added. The resulting silicate consisted of ~20 wt% glass and 80 wt% crystallized enstatite. Table 2 lists the bulk composition of the three starting silicates and the composition of the glass and enstatite from series II. The EMP analyses show small amounts of CaO in the glass, which must have been introduced by impurities in the starting chemicals. For use in the experiments, the hard silicate was crushed and powdered in an Fe-mortar, which led to minor Fe contamination, as can be seen from the analyses of the run products. Commercially available CaS (Alfa-Johnson Matthey) was used in the experiments, and the purity of the CaS was checked by x-ray diffraction. The x-ray pattern of CaS showed good agreement with the Powder Diffraction File (PDF) data (PDF 8-464) for crystalline CaS.

About 200 mg of the silicate starting material and 200 mg of sulfide were used in each experiment. The powdered starting materials (<100 μm) were equilibrated at 1200–1300 °C in evacuated silica tubes for varying time periods. Most samples in the 'FeS'/silicate system were placed directly in the silica tubes. Several 'FeS'/silicate experiments were done under more reducing conditions by placing some samples in corundum or mullite crucibles, which were surrounded by Al-foil as an O getter. The crucible and Al-foil were then placed into silica tubes and evacuated. All CaS/silicate experiments were done by placing the well-mixed charges into mullite crucibles, which were placed into silica tubes and then evacuated. The duration of the experiments was limited by the stability of the silica tubes at 1200 or 1300 °C, especially under more reducing conditions. After the experiments, the silica tubes were cooled in air. The tubes used for experiments under more reducing conditions often expanded in volume. This expansion was probably due to the evolution and expansion of S vapor during heating. After removal from the furnace, the tubes became fairly brittle, and the tubes containing reduced charges preferentially tended to implode during cooling. Quenching of the experimental charges in ice water was not done, because the CaS samples quickly dissolve and react away in water after implosion of the tubes.

The 'FeS' and CaS-bearing charges were mounted and sectioned for EMP analyses. The sulfide and silicate in the 'FeS'-bearing charges were separated for INAA. The sulfide and silicate in the CaS-bearing charges could not be separated and thus were not analyzed by INAA. All sample sections were prepared by cutting and polishing the samples in oil because water would oxidize or dissolve the sulfides. The INA analyses were done by irradiating 5–80 mg of sulfide and 3–20 mg of silicate in polyethylene capsules at the TRIGA Mark II reactor of the Johannes Gutenberg-Universität Mainz. Gamma ray counting procedures and evaluation of the gamma spectra were done by using the standard methods of the Mainz cosmochemistry group (*e.g.*, Wänke *et al.*, 1977). Electron microprobe analyses were done with the CAMECA SX50 electron microprobe at the Lunar and Planetary Laboratory in Tucson. The REE were analyzed using ZAF correction procedures and the REE standards of Drake and Weill (1972). About five to ten analyses of each phase were performed.

TABLE 2. Composition of starting silicates (Series I-III) for REE CaS/silicate partitioning experiments and silicate portion of EH- and EL-chondrites.

	Series I Bulk	Series II Bulk	Series II Glass*	Series II Enst.*	Series III Bulk	EH†	EL†
MgO	35.35	34.97	12.11	40.59	35.04	30.78	34.61
Al_2O_3	2.35	2.26	9.84	<0.12	2.22	2.68	2.94
SiO_2	60.45	58.13	60.17	59.84	58.10	62.56	58.93
CaO	0	0	1.60	<0.02	0	2.08	2.09
TiO_2	0.22	0.21	0.41	<0.05	0.21	0.13	0.14
Na_2O	1.05	1.01	1.97	<0.04	1.01	1.61	1.17
K_2O	0.19	0.19	0.51	0	0.19	0.17	0.13
La_2O_3	0	0	0	0	1	480 ppb	330 ppb
Sm_2O_3	0	0.96	4.76	<0.026	0	284 ppb	232 ppb
Eu_2O_3	0	0.93	4.55	<0.025	0	109 ppb	93 ppb
Gd_2O_3	0	0.97	4.60	<0.029	0	432 ppb	183 ppb
Yb_2O_3	0	0	0	0	0.89	319 ppb	278 ppb
Lu_2O_3	0	0	0	0	0.98	48 ppb	40 ppb
Total	100.0	100.0	100.60	99.89	100.0	100.0	100.0

wt% if not noted otherwise.
Series I: REE free silicate for reversal experiments.
Series II: Silicate spiked with Sm, Eu, and Gd.
Series III: Silicate spiked with La, Yb, and Lu.
*Bulk silicates consist of ~80 wt% enstatite and 20 wt% glass after fusion in all series (I, II, III). The composition of the enstatite and glass in silicate from series II are listed as a represenative example.
†Silicate portion of enstatite chondrites renormalized to 100% (Wasson and Kallemeyn, 1988), with all Ca and REE calculated as oxides.

RESULTS

All analytical results and REE partition coefficients are listed in Tables 3–5. The partition coefficients are expressed as weight ratios of concentration in sulfide over concentration in silicate phase analyzed.

The 'FeS'/Silicate System and REE 'FeS'/Silicate Partition Coefficients

The charges from the 'FeS'/silicate experiments resulted in 'FeS' or Fe-metal bearing 'FeS' spherules and silicate glass, which were easily separated for further analyses. Instrumental neutron activation analyses data for REE partitioning experiments between 'FeS' and basalt or 'FeS' and initially Fe-free oxide melt are listed in Table 3a. All experiments listed in Table 3a were done without Al-foil as an O getter. The results from experiments using either the tholeiitic basalt or the 'oxide'- melt are very similar. Table 3b gives INAA results for experiments under more reducing conditions, where Al-foil was included. The 'FeS'/silicate partition coefficients are displayed in Fig. 1.

Generally, REE 'FeS'/silicate partition coefficients decrease from light to heavy REE, except for Eu, which partitions about ten times stronger into the sulfide than neighboring Sm or Gd. Experiments conducted under more oxidizing conditions (runs without Al-foil as an O getter, discussed in the section on the calculation of fO_2 and fS_2 below) show lower REE 'FeS'/silicate partition coefficients. Results from INAA give the bulk composition of the segregating metal-sulfide phase. Partition coefficients for experiments where three phases coexist (metal, sulfide, silicate) must be regarded as (Fe + 'FeS')/(bulk silicate) partition coefficients. Thus REE partition coefficients for (pure 'FeS')/silicate must be larger than the (Fe + 'FeS')/silicate partition coefficients because of dilution of the 'FeS' phase with Fe-metal in the latter.

TABLE 3a. Experimental conditions, concentrations of REE in 'FeS' and silicate, and REE 'FeS'/silicate partition coefficients (D).

Run	EQ6			EQ1			VQ1			VQ2			VQ4			VQ3		
T (°C)	1200			1210			1200			1200			1200			1200		
Time (hrs)	2			1			2			2			2			5		
Silicate *	Tholeiitic Basalt + REE			Tholeiitic Basalt + REE			Fe-free Glass + REE			Fe-free Glass + REE			Fe-free Glass+REE			Fe-free Glass + REE		
X_{FeO}sil.†	0.049			0.056			0.047			0.053			0.081			0.064		
X_S sulf.‡	0.574			0.570			0.567			0.532			0.495			0.471		
aFe	n.a.			n.a.			n.a			n.a.			0.06			0.35		
log fO_2§	–9.6			–9.5			–9.7			–9.6			–11.7			–13.4		
log fS_2§	0			0			0			–0.57			–3.2			–4.4		
	'FeS'	Sil.	D#	'FeS'	Sil.	D#	'FeS'	Sil.	D#	'FeS'	Sil.	D#	'FeS'	Sil.	D#	'FeS'	Sil.	D#
Fe wt%	56.12	4.32	13	57.06	5.06	11.3	58.35	4.01	14.6	60.35	4.61	13.1	63.84	7.32	8.70	66.07	5.52	12
Sc ppm	<0.07	22.4	<0.003	<0.04	24.9	<0.002	–	–	–	–	–	–	–	–	–	–	–	–
La ppm	1.76	175	0.01	1.94	217	0.009	4.45	293	0.015	1.73	312	0.0056	0.94	227	0.0041	0.36	282	0.0013
Pr ppm	5.42	522	0.01	6.5	734	0.009	16.7	1060	0.016	6.60	1100	0.006	2.9	822	0.0035	1.2	1030	0.0012
Nd ppm	–	–	–	5.7	763	0.0075	15	904	0.017	7.30	913	0.008	–	–	–	–	772	–
Sm ppm	0.50	53.5	0.009	0.21	38.0	0.0055	0.41	28.4	0.014	0.13	28.5	0.0046	0.09	24.4	0.0037	0.04	31.7	0.0013
Eu ppm	1.25	19.3	0.065	1.29	29.5	0.044	2.55	38.8	0.066	1.70	44	0.039	0.2	33.6	0.0060	0.37	53	0.007
Gd ppm	5.70	1070	0.005	7.0	1200	0.0058	22.6	1570	0.014	4.70	1630	0.003	3.5	1250	0.0028	–	1410	–
Tb ppm	0.42	156	0.0027	0.72	206	0.0035	3.8	291	0.013	0.95	315	0.003	0.95	264	0.0036	–	277	–
Dy ppm	<0.07	42.6	<0.002	0.15	54.5	0.0028	1.05	78	0.014	0.29	85.8	0.0034	0.21	61	0.0034	<0.08	85.5	<0.001
Ho ppm	0.083	53.3	0.0016	0.11	46.8	0.0023	1.1	113	0.010	0.33	113	0.0029	0.3	85.9	0.0035	<0.12	99	<0.001
Yb ppm	0.24	164	0.0015	0.25	173	0.0014	4.50	332	0.014	1.05	349	0.003	0.79	248	0.0032	<0.27	313	<0.001
Lu ppm	0.088	24.8	0.0036	0.06	36.9	0.0016	0.78	49.9	0.016	0.17	50.6	0.0034	0.12	38.6	0.0031	0.047	44.3	0.001

Instrumental neutron activation analyses data for 'FeS' and silicate.
*Starting silicate used.
†Mole fraction of FeO in the silicate after the experiment.
‡Mole fraction of S in the sulfide after the experiment. Mole fraction of S is defined so that $X_{Fe}+X_S = 1$.
§Fugacities estimated from phase assemblages after the experiment as described in the text.
#Partition coefficient D = (concentration of element in the sulfide)/(concentration of element in the silicate).
n.a. = Not applicable.

TABLE 3b. Experimental conditions, concentrations of REE in 'FeS' and silicate, and REE Fe-S/silicate partition coefficients (D) in runs containing Al–foil as an O getter.

Run	EQ9			EQ10			EQ4			EQ3			QR1			QR2		
T (°C)	1200			1200			1200			1200			1200			1200		
Time (hrs)	5			5			2			2			2			2		
Silicate*	Tholeiitic Basalt + REE			Tholeiitic Basalt + REE			Tholeiitic Basalt + REE			Tholeiitic Basalt + REE			Tholeiitic Basalt			Tholeiitic Basalt		
X_{FeO} sil.†	0.042			0.039			0.106			0.109			0.026			0.042		
X_S sulf.‡	0.513			0.231			0.472			0.484			0.583			0.541		
aFe	1			1			0.35			0.18			n.a			n.a.		
log fO_2§	–14.7#			–14.8#			–12.0			–12.3			–10.2			–9.8		
log fS_2§	–5.8#			–5.8#			–4.4			–3.8			0			0		
	'FeS'#	Sil.	D$	'FeS'	Sil.	D$	'FeS'	Sil.	D$	'FeS'	Sil.	D$	'FeS'	Sil.	D$	'FeS'	Sil.	D$
Fe wt%	62.33	3.68	16.9	61.0	3.59	17	66.11	9.57	6.9	64.89	9.73	6.7	55.5	2.2	25.2	59.6	3.7	16.2
Sc ppm	<0.2	25.6	<0.007	<0.085	24.2	<0.004	<0.12	20.7	<0.006	<0.09	21.9	<0.004	<0.04	26.7	<0.0015	<0.08	24.1	< 0.003
La ppm	41	140	0.29	74.1	156	0.48	0.28	195	0.0014	0.13	221	0.0006	1.34	42.8	0.031	1.4	37.3	0.038
Pr ppm	142	433	0.33	280	545	0.51	0.7	686	0.001	–	753	–	–	–	–	–	–	–
Nd ppm	80	326	0.25	205	536	0.38	<32	692	–	–	710	–	–	–	–	–	–	–
Sm ppm	4.7	27.9	0.17	8.8	43.3	0.20	0.028	38.2	0.0007	<0.012	34.6	<0.0004	0.13	8.2	0.016	0.19	7.5	0.025
Eu ppm	10.5	12.3	0.85	16.5	15.3	1.08	0.096	27.6	0.0035	0.12	40.4	0.003	0.23	2.0	0.115	0.27	1.65	0.164
Gd ppm	66	818	0.081	155	1080	0.14	<4	1120	<0.0036	–	1140	–	–	–	–	–	–	
Tb ppm	10	162	0.062	21	222	0.094	<0.5	178	<0.0028	–	190	–	–	–	–	–	–	–
Dy ppm	2.6	44.7	0.058	3.1	37.8	0.082	<0.027	34	<0.0007	<0.03	40	<0.0007	–	–	–	–	–	–
Ho ppm	1.53	58.8	0.026	1.9	39.6	0.048	–	39	–	–	44.2	–	–	–	–	–	–	–
Yb ppm	5.7	175	0.033	5.7	181	0.032	<0.2	156	<0.0012	<0.14	161	<0.0009	–	–	–	–	–	–
Lu ppm	0.31	26.2	0.012	0.48	37.5	0.013	0.14	31.7	0.0044	<0.04	34.6	<0.001	–	–	–	–	–	–

Instrumental neutron activation analyses data for 'FeS' and silicate.
*Starting silicate used.
†Mole fraction of FeO in the silicate after the experiment.
‡Mole fraction of S in the sulfide after the experiment. Mole fraction of S is defined so that $X_{Fe} + X_S = 1$.
§Fugacities estimated from phase assemblages after the experiment as described in the text.
#Analytical data for sulfide exsolved from Si-bearing Fe-metal, fO_2 is lower limit (see text). The fO_2 is calculated from metal-silicate equilibrium. The fS_2 is calculated from metal-sulfide equilibrium.
$Partition coefficient D = (concentration of element in the sulfide)/concentration of element in the silicate).
n.a. = Not applicable.

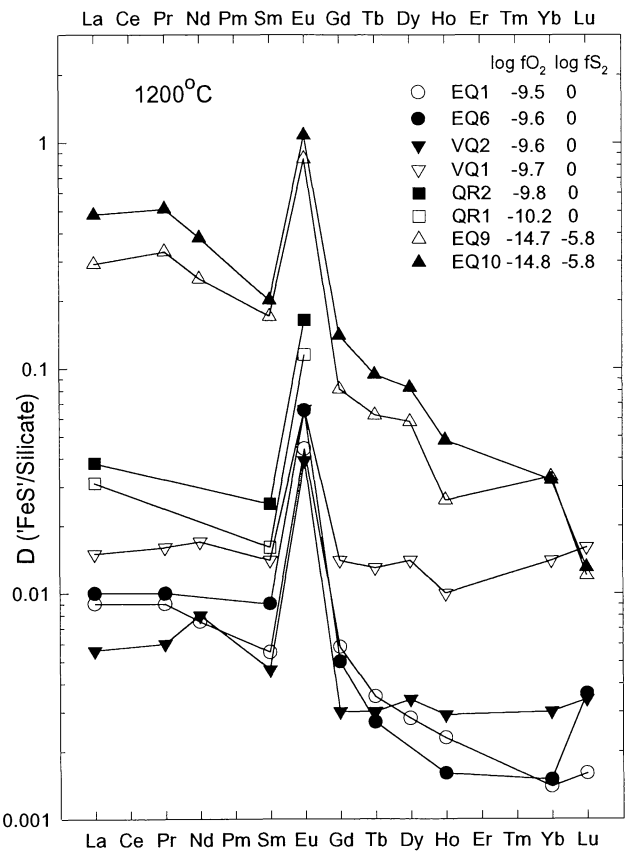

FIG. 1. Rare-earth-element 'FeS'/silicate partition coefficients for varying fO_2 and fS_2 at 1200 °C. Partition coefficients decrease from light to heavy REE, except for Eu, which shows preferential incorporation into Fe sulfide when compared to neighboring Sm and Gd. The experimental data are from Tables 3a and 3b.

Experiments done with basalt and REE concentrations suitable for EMP show similar results. These data are listed in Table 4. Experiments conducted at 1200 °C under more reducing conditions led to minor amounts of plagioclase formation in the silicate. This effect was not observed in experiments without Al-foil as an O getter. Plagioclase is a potential sink for the REE, especially Eu, as is well known from the literature (*e.g.*, Drake and Weill, 1975). If plagioclase is present, the REE partition coefficients calculated from the bulk silicates of reduced experiments analyzed by INAA must be interpreted as (Fe + 'FeS')/(matrix + plagioclase) partition coefficients. Because the plagioclase leads to more Eu (and other REE) in the bulk silicate, the 'FeS'/matrix partition coefficients are expected to be somewhat higher than those for (Fe + 'FeS')/(matrix + plagioclase). Table 4 lists calculated 'FeS'/ matrix partition coefficients from the EMP analyses of the matrix. These data show that under comparable O and S fugacities, REE 'FeS'/matrix partition coefficients are slightly higher (runs FEA and FYA) than the 'FeS'/bulk silicate partition coefficients (runs QR1 and QR2).

The EMP analyses of the 'FeS' from samples with high REE concentrations (~1 wt% in 'FeS') turned out to be complicated because the REE are inhomogeneously distributed in the sulfide phase and therefore the sulfides were analyzed by INAA (Table 4). The inhomogeneous distribution of REE in Fe sulfide is illustrated in Fig. 2 for an experiment where both 'FeS' and CaS were present (run CED in Table 5). Shown are single spot analyses for Eu and Sm in CaS and 'FeS', respectively. The Sm and Eu data for CaS show a

TABLE 4. Partitioning experiments between 'FeS' and tholeiitic basalt at high REE concentrations suitable for EMP analysis.

Run	FYA*	FYC*		FEA†	FEB†
T (°C)	1190	1291		1196	1203
Time (hrs)	15	15		16	17
X_{FeO} matrix‡	0.014	0.004		0.005	0.012
X_S sulf.§	0.540	0.526		0.544	0.513
log fO_2#	−10.8	−11.9		−11.6	−12.3
log fS_2#	0	−0.55		0	−1.4
wt%			'FeS' (INAA)		
Fe	59.28	60.80	Fe	58.74	62.20
Na	0.163	0.140	Na	0.202	0.040
K	0.075	0.048	K	0.190	0.027
Mn	0.038	0.010	Mn	0.024	0.107
La	0.279	0.156	Sm	0.155	0.004
Yb	0.032	0.032	Eu	0.322	0.071
Lu	0.076	0.012	Gd	0.155	0.005
wt%			Matrix (EMP)		
SiO_2	54.15	59.19	SiO_2	56.09	50.99
Al_2O_3	13.57	11.05	Al_2O_3	14.07	14.45
CaO	10.80	8.50	CaO	9.65	11.89
MgO	7.53	10.53	MgO	7.67	9.04
TiO_2	2.18	1.44	TiO_2	1.64	2.96
Na_2O	0.15	0.83	Na_2O	0.73	0.95
K_2O	0.16	0.78	K_2O	0.60	0.89
FeO	1.45	0.41	FeO	0.53	1.26
La_2O_3	2.19	1.51	Sm_2O_3	3.30	2.81
Yb_2O_3	4.39	1.95	Eu_2O_3	0.89	1.56
Lu_2O_3	3.34	1.99	Gd_2O_3	4.34	3.01
Total	99.91	98.18	Total	99.51	99.81
other phases$	en, an	–		en	dio
D(La)@	0.15	0.12	D(Sm)@	0.054	0.0017
D(Yb)@	0.008	0.019	D(Eu)@	0.419	0.053
D(Lu)@	0.026	0.007	D(Gd)@	0.041	0.0019

*Experiments with La, Yb, and Lu.
†Experiments with Sm, Eu, and Gd.
‡Mole fraction FeO of silicate matrix after the experiment.
§Mole fraction of S in Fe sulfide phase after experiment. Mole fraction of S is defined so that $X_{Fe} + X_S = 1$.
#Fugacities are estimated from phase assemblages after the experiment.
$Other phases present in the silicate: An = anorthite; dio = diopside; en = enstatite; no other phase observed.
@Partition coefficient D = (concentration of element in sulfide)/(concentration of element in silicate matrix). Note the necessary conversion from oxide to element for computing partition coefficients.

relatively homogeneous distribution (4–6% variation) while the data for 'FeS' spread more significantly and make it difficult to obtain a representative analyses. The different solid solution behavior of the REE in 'FeS' and CaS may be understood by comparing the FeS-CaS and FeS-EuS phase diagrams. The literature phase diagrams are shown in Fig. 3. The FeS and CaS phase relations show that there is almost no solid solubility of CaS in FeS (*e.g.*, Skinner and Luce, 1971). EuS is chemically very similar to CaS, and similar behavior is expected in the EuS-FeS system. Meyer and Pink (1973) note that the solid solubility of EuS in FeS, if any, is very small. The inhomogeneous distribution of the REE in 'FeS' is most likely due to REE sulfide exsolution from 'FeS' during cooling, so that EMP analyses of the REE in 'FeS' are more unreliable than the bulk analyses of 'FeS' by INAA, which integrates the concentration over the whole sample. Replicate INA analyses of 'FeS' from

TABLE 5. Experimental conditions, concentrations of REE in CaS and silicate, and REE CaS/silicate partition coefficients.

Run	CYA*	CYC*	CYB*		CEI† (Rev.)	CEC‡	CEE‡	CEH† (Rev.)	CED‡§
T (°C)	1202	1306	1308		1202	1273	1295	1304	1308
Time (hrs)	18	21	20		18	16	16	22	26
log fO_2/fS_2#	−7.6	−7.2	−7.2		−7.6	−7.2	−7.1	−7.2	−6.9
wt%				Oldhamite					
Ca	51.80	48.67	47.46	Ca	49.31	50.31	49.91	48.53	52.97
Mg	1.76	4.4	4.83	Mg	0.11	2.27	2.40	3.62	0.46
Fe	0.30	0.92	1.04	Fe	0.37	0.69	0.88	0.92	1.88
Na	0.12	0.11	0.09	Na	0.10	0.08	0.09	0.19	0.09
S	42.36	43.52	43.17	S	43.64	41.23	41.70	44.75	44.58
La	0.39	0.15	0.21	Sm	0.75	0.53	0.55	0.79	0.42
Yb	0.43	0.46	0.52	Eu	0.83	0.68	0.78	1.04	0.49
Lu	0.39	0.42	0.45	Gd	0.71	0.48	0.51	0.99	0.41
Total	97.55	98.65	97.77	Total	95.82	96.27	96.82	100.8	101.3
$X_{CaS}$$	0.943	0.860	0.845	$X_{CaS}$$	0.940	0.923	0.916	0.880	0.962
$X_{MgS}$$	0.053	0.128	0.142	$X_{MgS}$$	0.055	0.068	0.073	0.108	0.014
$X_{FeS}$$	0.004	0.012	0.013	$X_{FeS}$$	0.005	0.009	0.012	0.012	0.024
wt%				Silicate Matrix					
SiO_2	52.04	45.39	47.23	SiO_2	54.27	50.84	52.96	47.32	57.78
Al_2O_3	11.03	21.43	19.71	Al_2O_3	11.58	10.29	10.30	16.83	6.48
CaO	15.75	15.30	14.68	CaO	16.20	20.38	18.91	14.76	23.11
MgO	8.12	15.16	15.68	MgO	8.69	11.72	10.88	17.42	6.51
TiO_2	0.79	0.31	0.32	TiO_2	0.96	0.99	1.24	0.28	1.39
Na_2O	0.17	0.19	0.20	Na_2O	0.10	0.08	0.13	0.17	0.23
K_2O	0.18	0.16	0.18	K_2O	0.145	0.08	0.14	0.15	0.28
FeO	0.06	0.14	0.13	FeO	<0.03	0.18	0.14	0.10	0.59
La_2O_3	3.68	0.44	0.46	Sm_2O_3	2.15	1.83	1.88	0.75	0.89
Yb_2O_3	3.39	0.37	0.36	Eu_2O_3	0.52	0.68	0.80	0.56	0.50
Lu_2O_3	3.35	0.40	0.42	Gd_2O_3	2.29	1.69	1.76	0.92	0.98
Total	98.56	99.29	99.37	Total	96.91	98.76	99.14	99.26	98.74
X_{CaO}@	0.191	0.168	0.159	X_{CaO}@	0.188	0.228	0.209	0.159	0.253
X_{FeO}@	0.0006	0.0012	0.0011	X_{FeO}@	0.0003	0.0016	0.0012	0.0008	0.0033
other phases¤	en	–	–		en	en	dio	–	–
D(La)¥	0.12	0.41	0.52	D(Sm)¥	0.45	0.34	0.34	1.23	0.55
D(Yb)¥	0.14	1.44	1.57	D(Eu)¥	1.87	1.13	1.14	2.16	1.14
D(Lu)¥	0.13	1.04	1.20	D(Gd)¥	0.36	0.33	0.34	1.24	0.48

*Starting silicate spiked with La, Yb, and Lu (Series II in Table 2).
†Starting silicate is REE free (Series I in Table 2). "Rev." indicates that REE were initially contained in CaS.
‡Starting silicate contains Sm, Eu, and Gd (Series III in Table 3).
§Experiment also contains FeS.
#Fugacity ratio estimated from CaS/CaO concentrations, see text.
$Mole fraction in oldhamite.
@Mole fraction in silicate matrix.
¤Other phases present in the silicate: dio = diopside; en = enstatite; no other phase observed.
¥Partition coefficient D = (concentration of element in sulfide)/(concentration of element in silicate matrix). Note the necessary conversion from oxide to element for computing partition coefficients.

individual runs resulted in no differences in REE concentrations (with absolute concentrations of different REE ranging from 10 to 1000 ppm) within gamma counting statistics. In addition, the lower bulk REE concentrations in experiments designed for INAA (*e.g.*, 15 ppm Eu) may also preclude REE exsolution from the 'FeS', while samples containing percent levels of REE (*e.g.*, ~1 wt% Eu) are more likely to exsolve EuS from 'FeS' during cooling.

Calculation of O and S Fugacities in the 'FeS'/Silicate System–It is necessary to know the oxygen and sulfur fugacities during the experiment to apply the measured partition coefficients to natural systems. As in the other previous studies (Jones and Boynton, 1983; Dickinson *et al.*, 1990a,b, 1991), no direct measurement of the fO_2 and fS_2 was possible because samples were equilibrated in evacuated silica tubes. Unlike experiments which utilize gas-mixtures in open (flow) systems to superimpose fO_2 or fS_2 on experimental charges, the fugacities in equilibrium with the samples here were controlled by the sample compositions, and in particular, by the amount of S added. During the experiment, silicate and sulfide, and in some cases metal, coexist. The fO_2 and fS_2 can then be estimated from the phase compositions after the experiment. In some experiments, Al-foil was added separately as an O getter to lower the fO_2. However, the Al-foil also reacted with S, and the fO_2 of the Al-Al_2O_3 buffer was not reached. The fugacities for these runs were also calculated from the resulting phase assemblages.

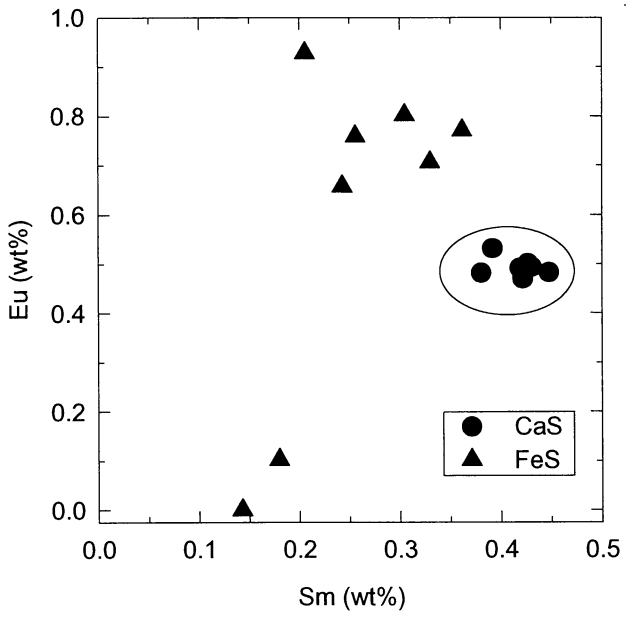

FIG. 2. Electron microprobe spot analyses of Sm and Eu in a sample containing CaS and FeS (sample CED in Table 5). The data obtained in FeS scatter significantly while measurements in CaS yield data which are consistent within ± 4–6%. The scatter in FeS can be explained by exsolution of the REE from FeS during quenching, while REE remain dissolved in CaS. See text for details.

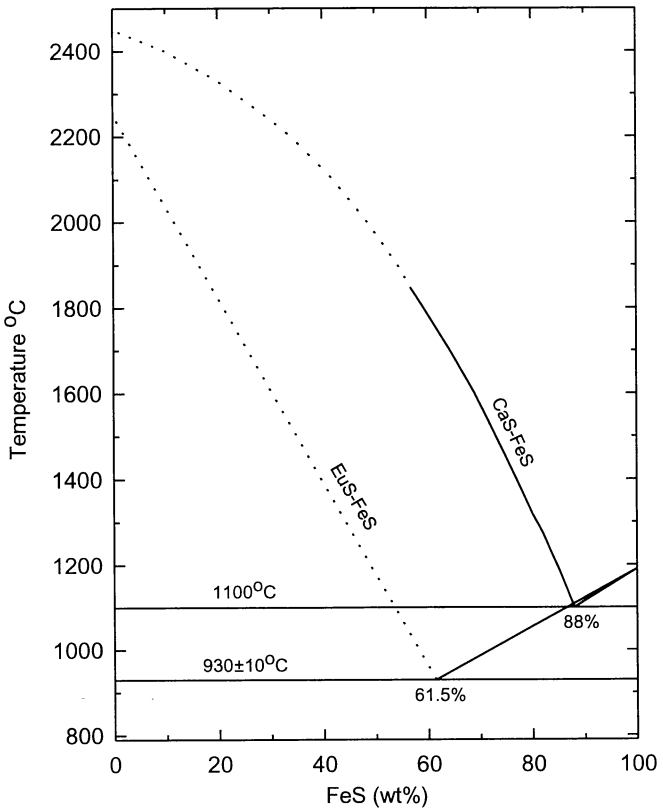

FIG. 3. The FeS-CaS and FeS-EuS phase diagrams (after Vogel and Heumann, 1941; Heuman, 1942; Meyer and Pink, 1973). Dotted lines are extrapolated to the melting points (Medvedev *et al.*, 1979; Gmelin *et al.*, 1983). Below the eutectic temperatures, almost no solubility of EuS or CaS in FeS occurs.

The calculation of the O and S fugacities in the 'FeS' bearing experiments is the same as discussed earlier for similar partitioning experiments on Mo and W (Lodders and Palme, 1991).

Depending on the amount of S added to the experimental charges, three different types of phase assemblages are possible at run temperature. If we define the mole fraction of S (X_S) in the bulk (metal-) sulfide phases of the run products so that $X_{Fe} + X_S = 1$, we can use the phase relations of the Fe-S system (Kubaschewski, 1982) to determine the coexisting phases (other than gas phase) at run temperature. At 1200 °C, the three possible types of phase assemblages are: (1) Three coexisting phases: silicate melt, solid Fe-metal and Fe-rich 'FeS' for $X_S < 0.385$; (2) two coexisting melts: silicate melt and Fe-rich 'FeS'-melt (for $0.385 < X_S < 0.5$); and (3) two coexisting melts: S-rich 'FeS' melt (for $X_S > 0.5$) and silicate melt. Literature data for S fugacities above Fe-sulfide melts as a function of composition, (*i.e.*, X_S) have been compiled and assessed by Schürmann and Henke (1972). The mole fraction of S in the bulk (metal)-sulfide was calculated after the experiment. The fS_2 over (metal bearing)-sulfide melts at run temperature was then derived using the X_S-fS_2 relations from the literature (see Fig. 1 in Lodders and Palme, 1991).

The O fugacity (fO_2) was calculated by assuming ideal solution of FeO in the silicate, so that the activity of FeO (a_{FeO}) equals the mole fraction of FeO (X_{FeO}) in the silicate. Turkdogan (1983) summarized experimentally determined FeO activities, and these data suggest that the FeO activity coefficients in silicate melts are close to unity. The fO_2 was calculated from the equation:

$$\log fO_2 = 2\,[\log X_{FeO} - \log a_{Fe} - \log K_{IW}] \qquad \text{Eq. (1)}$$

where K_{IW} is the temperature dependent equilibrium constant for the iron-wüstite buffer ($\log K_{IW} = -3.416 + 13834/T$ for 1184–1665 K; Kubaschewski and Alcock, 1979) and a_{Fe} is the activity of Fe. In the case where three phases (metal, sulfide, and silicate melt) are present during the experiment, the activity of Fe metal (a_{Fe}) equals one, and the fO_2 is only a function of the FeO concentration of the silicate. In experiments where Al-foil was included as an O getter to obtain more reducing conditions, metal can contain Si and the activity of Fe is less than one. In principle, the reaction Si (in Fe metal) + O_2 = SiO_2 (in melt) could be used to calculate the fO_2 of these samples. Although the activity of Si in Fe metal is known, SiO_2 activities in silicate melts are more uncertain. Also, INAA is not sensitive to measure Si. Quenching will also alter the Fe-Si-S bearing phases as was observed by the exsolution of 'FeS' from the Si-bearing metal in experiments EQ9 and EQ10. The listed fO_2 values were calculated from Eq. (1) assuming $a_{Fe} = 1$ and give only upper bounds of the fO_2 for these experiments. Taking $a_{Fe} \sim 1$ is a reasonable assumption for samples with low concentrations of Si in the metal.

In the second case, where solid Fe metal is absent and Fe-rich 'FeS' melt and silicate melt are present during the experiment, the Fe-activity data from Stofko *et al.* (1974) were used to calculate the fO_2 from Eq. (1). The activity data, together with the fO_2 and fS_2, are listed in Tables 3 and 4.

The O fugacity in the third case, with S-rich FeS melt and silicate melt, was obtained using the reaction:

$$\text{FeO (silicate)} + 0.5\ \text{S2 (g)} = \text{FeS (sulfide)} + 0.5\ \text{O2 (g)} \qquad \text{Eq. (2)}$$

Once the fS_2 is derived from the Fe-S phase relations, the fO_2 can be calculated from:

$$\log fO_2 = 2[\log K_2 - \log a_{FeS} + \log X_{FeO}] + \log fS_2 \quad \text{Eq. (3)}$$

where the activity of the pure FeS melt is taken $a_{FeS} = 1$. The data to calculate the equilibrium constant ($K_2 = K_{FeS}/K_{IW}$) were taken from the JANAF Tables (1985) and Kubaschewski and Alcock (1979).

The CaS/Silicate System and REE CaS/Silicate Partition Coefficients

Analytical results and REE partition coefficients between CaS and silicate are listed in Table 5 and displayed in Fig. 4. Oldhamite-bearing samples spiked with Sm, Eu, and Gd for EMP analyses appear pinkish after the experiment, while samples containing La, Yb, and Lu appear greenish. In all experiments, small CaS grains and aggregates were surrounded by silicate glass. X-ray patterns obtained from the samples are similar to those of the synthetic CaS used and show the presence of crystalline CaS. The melting point of pure CaS is 2450 ± 50 °C (Medvedev *et al.*, 1979), so that no CaS melt is expected at run temperatures of 1200–1300 °C. The larger CaS aggregates probably formed by sintering. The silicate melt acts as a sintering aid (*e.g.*, Kingery *et al.*, 1976) and promotes growth of the CaS aggregates. The introduction of Mg (up to 5 wt%) into CaS is explained by exchange reactions of CaS and silicate melt during sintering. Although the starting silicates are essentially CaO-free before the experiment, the matrix can contain up to 15 wt% CaO after equilibration with CaS. Before the experiment, the REE were concentrated in the glass of the starting silicate, which made up ~20 wt% of the bulk silicate. The enstatite in the starting silicate did not contain any significant amounts of REE. During the experiment, the amount of enstatite decreased and the amount of melt increased by incorporation of Ca from the CaS. Experiments conducted at 1200 °C also contain enstatite crystals in the silicate matrix, but enstatite was not present after heating at 1300 °C.

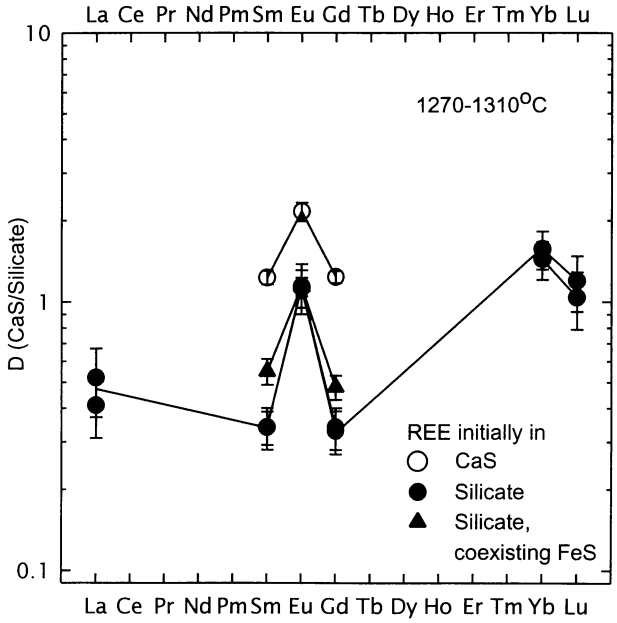

FIG. 4. Rare-earth-element CaS/silicate partition coefficients for temperatures between 1270 °C and 1310 °C. Europium shows preferential incorporation into CaS when compared to Sm and Gd. Partition coefficients for La are smaller than that of Yb and Lu. Note that La, Yb, and Lu were grouped together in the same charges. Experiments where the REE were initially contained in CaS show values 2–4 times higher than those obtained from experiments where the REE were initially contained in the silicate. Although equilibrium was not reached, the partition coefficients are much lower than the value of ~100 needed to explain magmatic incorporation of the REE into oldhamite in aubrites. The data are from Table 5.

Rare-earth-element partition coefficients at temperatures between 1270–1310 °C show an increase from light to heavy REE (DLa ~ 0.5 to DLu ~ 1.1), with the exception of Eu (Fig. 4). Europium shows a preferential incorporation into CaS (DEu ~ 1.2) when compared with neighboring Sm and Gd. The partitioning behavior of Eu between CaS and silicate is similar to Eu partitioning between 'FeS' and silicate. However, the overall trend for REE partitioning into CaS is an increase in D values from LREE to HREE. This trend is opposite to that found for REE partitioning between 'FeS' and silicate (D values decrease from LREE to HREE).

Experiments that were conducted with REE-spiked CaS and initially REE free silicate show similar results to experiments where the REE had to move from the silicate into CaS. However, the CaS/silicate partition coefficients for these 'reversal' experiments are higher (about a factor of 2 for Eu and ~4 for Sm and Gd), which indicates that equilibrium was not reached within the duration of the experiments. Thus, the results for the REE-spiked CaS experiments give upper limits for REE partitioning between CaS and silicate melt while experiments with REE-spiked silicate give lower limits. Unfortunately, longer experimental durations (>24 h) were hampered by the instability of the silica tubes used for containment of the charges. Nevertheless, the attempted reversal experiments demonstrate that the REE CaS/silicate partition coefficients are small and that the REE favor the silicate instead of CaS.

Calculation of O and S Fugacities in the CaS/Silicate System–The derivation of the O and S fugacities for the CaS/silicate experiments was more complicated than that for 'FeS'/silicate system described above. Because the CaS experiments were almost Fe-free, the 'FeS' phase relations could not be used for calculating the fO_2 and fS_2. The fugacities in the CaS experiments are determined by the reaction:

$$\text{CaO (silicate)} + 0.5\ S_2\ (g) = \text{CaS (sulfide)} + 0.5\ O_2\ (g) \quad \text{Eq. (4)}$$

A rough estimate of the fugacity ratio, fO_2/fS_2 was obtained by assuming ideal solution behavior of CaS in the sulfide and CaO in the silicate melt, or by assuming that the ratio of the activity coefficients $\gamma_{CaS}/\gamma_{CaO}$ is about one. The fugacity ratio is then given by:

$$\log \frac{fO_2}{fS_2} = 2\left[\log K_4 - \log \frac{X_{CaS}}{X_{CaO}}\right] \quad \text{Eq. (5)}$$

where the equilibrium constant K_4 was calculated from JANAF data and X represents the mole fractions of CaS in the sulfide and CaO in the silicate. Absolute calculations of the O fugacities would be possible if the S fugacity could be determined independently. However, unlike the Fe-S system discussed earlier, where the S fugacity over 'FeS' melts can be obtained from literature investigations, nothing is known about the S fugacities above CaS (bearing) sulfide. Therefore, only the ratio fO_2/fS_2 is listed in Table 5.

COMPARISON OF REE SULFIDE/SILICATE PARTITION COEFFICIENTS WITH LITERATURE DATA

An overview of other experimental determinations of 'FeS'/silicate and CaS/silicate partition coefficients is given in Table 6. Jones and Boynton (1983) report partitioning experiments for La, Gd, and Lu between 'FeS', (Ca,Mg)S, and basaltic melt. The overall trend that REE 'FeS'/silicate partition coefficients decrease from La

TABLE 6. Rare-earth-element sulfide/silicate partition coefficients: Comparison with other experimental data.

'FeS'/Silicate					
T (°C)	1200	1200	1200	1250	1250
Ref.	[1]	[2*]	[3]	[2]	[1]
La	1.8	–	0.39	–	0.76
Nd	–	–	0.32	–	–
Sm	–	–	0.19	–	–
Eu	–	0.9/2.4*	0.97	1	–
Gd	1.3	0.3/0.6	0.11	0.3	0.22
Yb	–	–	0.033	–	–
Lu	0.2	–	0.013	–	0.004

CaS/Silicate						
T (°C)	1200	1200	1250	1250	1300	1270–1310
Ref.	[1]	[2*]	[1]	[2*]	[2]	[3]
La	0.4	0.5	0.34	–	0.3	0.47
Ce	–	1	–	–	0.6	–
Nd	–	1.8/2*	–	2.5/4.5	1.2	–
Sm	–	3/3.5	–	3.5/3	1.8	0.34
Eu	–	0.8/2.2/1.8	–	1.8	1.2	1.13
Gd	12	4/2/3.5	2.5	8	2	0.34
Yb	–	6/4	–	9	3	1.5
Lu	24	–	1.7	–	–	1.1

[1] Jones and Boynton, 1983; J. Jones, pers. comm.
[2] Dickinson *et al.*, 1990a,b; 1991 (data were taken from figures).
[3] This work.
*Values separated by "/" indicate results obtained under different conditions.

to Lu and that REE CaS/silicate partition coefficients increase from La to Lu is similar to the results here. However, their absolute D values are ~10 times higher for 'FeS'/silicate and up to 20 times higher for the CaS/silicate data. These differences may be due to different fO_2 and fS_2 conditions. Jones and Boynton added Al metal into their charges, and they report a log $fO_2 \sim -17$. Their log fO_2 value was ~2.5 log units more reducing than the most reducing experiments reported here, which should lead to higher partition coefficients (see the next section). Unfortunately, the partitioning behavior of Eu was not studied by Jones and Boynton (1983).

Dickinson *et al.* (1990a,b, 1991) reported partitioning of Nd, Sm, Eu, Gd, and Yb between (Ca,Mg)S melt and silicate melt. Their partition coefficients are ~2–3 times higher than the present values. The exception is Eu, which was less concentrated in the (Ca,Mg)S than neighboring Sm and Gd. This behavior of Eu is opposite to that found in the experiments here, where Eu always preferentially enters the sulfide phase in comparison to Sm and Gd. These differences may be due to the different composition of the sulfide and silicate phases. The silicate used here was chosen to have enstatite chondritic silicate composition and thus contained less Al than the basaltic melt, which was used by Jones and Boynton (1983) and Dickinson *et al.* (1990a,b). In addition, Jones and Boynton (1983) and Dickinson *et al.* (1990a) added Al powder to the basalt to obtain a reduced melt. Dickinson *et al.* (1990a,b) speculate that plagioclase crystallization may have shifted the partitioning of Eu, because Eu is very compatible in plagioclase. However, if equilibrium was reached during the experiments by Dickinson *et al.* (1990a,b), crystallization of plagioclase should not have had any influence on the sulfide/silicate partition coefficients. If plagioclase formed during cooling of the charges, some Eu would be removed into the crystallizing plagioclase and Eu concentrations in the matrix would be lower, depending on the amount of plagioclase formed. In that case, CaS/matrix partition coefficients would appear to be higher than actual partition coefficients at silicate melt temperature. Experiments conducted by Dickinson *et al.* (1990b) without directly adding Al powder to the basalt yielded similar results, showing that Eu partitions less into (Ca,Mg)S than Sm and Gd. However, the melt compositions are not given in their abstract so a meaningful comparison of the data is difficult. Another system investigated by Dickinson *et al.* (1991) utilized a reduced aubritic silicate composition, which was produced from Mg and Al metal, together with SiO_2 and CaO. Sulfur was supplied by introduction of FeS_2 to the charge. The results of these experiments yielded partition coefficients similar to those reported earlier by Dickinson *et al.* (1990a,b).

A more likely explanation for the different trends in Eu partitioning is that the sulfide composition influences the REE partitioning (Lodders, 1995, 1996). The chemical behavior of Eu^{2+} is very similar to that of Ca^{2+}, and therefore Eu is expected to be preferentially incorporated into Ca-rich, Mg-poor sulfides relative to Mg-rich, Ca-poor sulfides. Stoichiometric CaS contains 55.55 wt% Ca, while the CaS in the reacted charges in this work contains ~48–50 wt% Ca and up to 5 wt% Mg. In contrast, the CaS in experiments by Dickinson *et al.* (1990a) contains ~30 wt% Ca and is thus more Mg-rich. Very recently, Dickinson and McCoy (1996) performed experiments similar to those by Dickinson *et al.* (1991) using an aubritic silicate composition and confirmed our explanation that the composition of the oldhamite indeed influences the partition coefficients (see also section on thermodynamic predictions of REE partition coefficients).

The differences between the sulfide composition in this study and in studies by others resulted from the different experimental approaches. The experimental design used here for CaS/silicate partitioning is similar to the experimental design of metal/silicate partition experiments. Generally metal and silicate are mixed and solid metal is equilibrated with a silicate melt at temperatures below the melting point of the metal (*e.g.*, Newson and Drake, 1983; Schmitt *et al.* 1989). The same approach was used here because the precursor material of the aubrite parent body already contains CaS (see also discussion section).

In contrast, in the experiments by Jones and Boynton (1983) and Dickinson and coworkers, CaS formed *in situ* by the sulfurization of CaO. The S was supplied by FeS_2, and the reduction of CaO was achieved by adding metallic Al or Mg to the charges. Thus reactions exemplified by:

$$CaO + 1/2\ FeS_2 + 2/3\ Al = CaS + 1/2\ Fe + 1/3\ Al_2O_3 \quad \text{Eq. (6a)}$$

or

$$CaO + 1/2\ FeS_2 + Mg = CaS + 1/2\ Fe + MgO \quad \text{Eq. (6b)}$$

took place. In addition, MgS formation via reactions such as:

$$CaO + Mg + FeS_2 = CaS + MgS + MgO + Fe \quad \text{Eq. (7a)}$$

or

$$CaO + Mg + FeS_2 + Al = CaS + MgS + Fe + Al_2O_3 \quad \text{Eq. (7b)}$$

must have occurred, because Mg-rich (Ca,Mg)S is also observed in their experiments. Thermodynamically, the sulfurization of Mg to MgS is less favorable than the formation of CaS and requires more reducing conditions. Equations (6) and (7) also explain why CaS is often associated with FeS or metal in the experiments by Jones and Boynton (1983), Dickinson (1990a), and Dickinson and McCoy (1996). Their experiments may be irrelevant to the differentiation process on the aubrite parent body since there probably was no metallic Mg or Al present on it.

Dickinson and McCoy (1996) also report that the (Ca,Mg)S produced in their experiments shows textures that indicate that (Ca,Mg)S liquids were present. However, these textures just as well may be replacement textures. At the experimental temperatures of 1200–1300 °C, pyrite decomposes and forms an FeS liquid, which supplies the S for the formation of (Ca,Mg)S (Eqs. 6a–7b). Nothing is known about the CaS-MgS phase relations at high temperatures, but the CaS-MnS phase diagram can provide a guide for the CaS-MgS system because both systems show similarities at temperatures up to 1100 °C (Skinner and Luce, 1971). In the CaS-MnS system, complete solid solubility exists from 1150 °C up to 1500 °C, where the minimum in the liquidus occurs at ~77 wt% MnS (Leung and van Vlack, 1979). Assuming that the CaS-MgS system is not that different at high temperatures, liquid (Ca,Mg)S is not expected at 1200–1300 °C. Because MgS (melting point >2000 °C) melts much higher than MnS (1610 °C), the stability field for CaS-MgS solid solutions may even extend to higher temperatures. Experimental investigation of the CaS-MgS and CaS-MgS-FeS systems at high temperatures are needed to resolve this issue.

If it could be established that liquid (Ca,Mg)S was present in the other studies, then this may be an explanation for the different Eu partitioning results found by Dickinson and co-workers (1990a,b, 1991, 1996) and in this study, where solid CaS is always present. One could speculate that solid CaS and silicate liquid approach equilibrium more slowly than liquid (Ca,Mg)S and silicate liquid. However, the 'reversal' experiments reported here give upper limits to the partition coefficients, and the trend of DEu > DSm = DGd is the same in 'normal' experiments. Thus, a closer approach to equilibrium is probably not the explanation for the different partitioning trend observed. No reversal experiments were reported by Dickinson *et al.* (1990a,b, 1991) or Jones and Boynton (1983) so that it is not clear whether their (Ca,Mg)S/silicate partition coefficients represent equilibrium values.

Another factor that may influence the partitioning is the O fugacity. Dickinson *et al.* (1990b) derive the fO_2 from the observed phase assemblages in a similar manner as done here. In their work, they qualitatively list the fO_2 in the experiments as either equal to, smaller than, or higher than the fO_2 for aubrites. However, they do not indicate which fO_2 and temperature they assume for aubrite formation. Dickinson *et al.* (1990b) found that DEu increases and DGd decreases with increasing O fugacity. These findings are somewhat surprising because more reducing conditions should stabilize the REE sulfides and thus lead to higher sulfide/silicate partition coefficients, as is seen from LeChatelier's principle and Eqs. 8a–8c discussed in the next section. Therefore, an increase of DEu with increasing fO_2 seems confusing. Dickinson *et al.* (1990b) report a similar confusing situation for the dependence of REE partition coefficients between 'FeS' and silicate: absolute values of DEu and DGd increase with increasing O fugacity, while in this study, decreasing DEu and DGd are observed with increasing fO_2 (Fig. 1). The next section describes thermodynamic calculations to predict the trends of REE partition coefficients between sulfides and silicates as a function of fO_2 and shows that partition coefficients are expected to decrease with increasing fO_2.

THERMODYNAMIC PREDICTIONS OF THE REE SULFIDE/SILICATE PARTITION COEFFICIENTS AND PHASE DIAGRAM STUDIES OF REE SULFIDES WITH CaS, MgS, AND FeS

Thermodynamic calculations are useful for predicting trends in REE partitioning between sulfides and silicates. The general exchange reaction of a lanthanide (M) between sulfide and silicate can be written as:

$$MO_{1.5}\ (\text{silicate}) + 0.5\ S_2 = MS\ (\text{sulfide}) + 0.75\ O_2 \qquad \text{Eq. (8a)}$$

or

$$MO_{1.5}\ (\text{silicate}) + 0.75\ S_2 = MS_{1.5}\ (\text{sulfide}) + 0.75\ O_2 \qquad \text{Eq. (8b)}$$

We also need to consider the reaction:

$$EuO\ (\text{silicate}) + 0.5\ S_2 = EuS\ (\text{sulfide}) + 0.5\ O_2 \qquad \text{Eq. (8c)}$$

The analogous reaction may also become important for Yb under very reducing conditions.

The REE are probably dissolved in the silicate in their trivalent state (M^{3+}) and are assumed to be present as sesquioxides (M_2O_3) for modeling purposes, although the actual dissolved species are unknown. For Eu, the divalent state (as EuO) was also considered because Eu is likely to be dissolved as Eu^{2+} under the reducing conditions of interest. Two possible types of REE sulfides, the monosulfides (MS) and the sesquisulfides (M_2S_3 or $MS_{1.5}$) were considered as stable sulfides, depending on the fS_2. In the 'FeS' experiments, the fS_2 is either above or close to the fS_2 above Fe-bearing 'FeS' liquids, and this fS_2 was also assumed for the CaS experiments. (Note that the fS_2 during differentiation in enstatite meteorites is determined by vapor pressure of S_2 above metal saturated FeS liquid.) To investigate whether the REE monosulfides or the REE sesquisulfides are relevant during partitioning, the fS_2 necessary to stabilize the sesquisulfide is calculated from the reaction:

$$MS + 0.75\ S_2 = MS_{1.5} \qquad \text{Eq. (9)}$$

and compared with the fS_2 above Fe-metal saturated sulfide melts. For all REE except Eu, it is found that the sesquisulfides are stable under this S fugacity at temperatures ~1200–1300 °C. Thus, partitioning of the REE sesquisulfides into CaS according to Eq. (8b) must be considered. In contrast, the sesquisulfides are unimportant during condensation of the REE-sulfides into CaS because the fS_2 in a highly reduced solar nebula (C/O ~ 1.2, P = 10^{-3} bars) is ~13 log-units below the fS_2 prevailing above Fe-saturated sulfide melts. The sesquisulfides are unstable at these low S fugacities (Lodders and Fegley, 1993). Europium sesquisulfide is unimportant because Eu_2S_3 is apparently nonexistent (Gmelin *et al.*, 1983). Only EuS is relevant for Eu extraction from silicate into sulfides.

Phase diagrams of REE-sulfides and CaS also indicate that the REE sesquisulfides are more important than the monosulfides, except for Eu, where the monosulfide is relevant. The data for the REE sulfide-CaS systems show that the REE and Y are dissolved in their trivalent state (*i.e.*, as sesquisulfides), forming solid solutions with CaS (for summaries, see Flahaut, 1979; Eliseev and Kuzmichyeva, 1990). In particular, the heavy REE and Y form solid solutions with CaS over a wide homogeneity range, but light REE solid solution with CaS is very limited. For example, Flahaut *et al.* (1961) found that Y_2S_3 shows a significant range of solid solubility in CaS. At higher Y concentrations of ~10–20 mol%, a distinct phase CaY_2S_4 containing Y^{3+} coexisted with CaS. Similar phase relations were found for the heavy REE-sulfides and CaS in other studies by Flahaut *et al.* (1963). Tsai and Meschter (1981) studied the solubility behavior of Y_2S_3, Dy_2S_3, Er_2S_3 and Yb_2S_3 in CaS at 800–1200 °C for REE sulfide concentrations up to 40 mol% at constant S fugacities of log fS_2 = –5.5. They found that the

sesquisulfides dissolved in CaS with relatively high solubilities up to 15–30 mol%. In general, the phase diagram studies were conducted under very reducing conditions, and the S fugacities used by Tsai and Meschter (1981) are comparable to the S fugacity above Fe-saturated sulfide liquids at 1200 °C.

In contrast EuS, and not Eu_2S_3, is dissolved in CaS (*e.g.*, Eliseev and Kuzmichyeva, 1990), as was also found by Mössbauer studies (*e.g.*, Wickman *et al.*, 1970). EuS and CaS form a continuous series of NaCl-type solid solutions (*e.g.*, Van Tien and Khodadad, 1970; Eliseev and Kuzmichyeva, 1990). However, Van Tien and Khodadad (1970) find that the difference in the metallic radii is too large to allow solid solution for the system MgS-EuS.

Studies of the REE-Mg-S system showed that the REE sesquisulfides are present in solid solution in MgS. As is the case for the REE-Ca-S system, the heavy REE have an extensive range of solid solubility in MgS, and at higher REE concentrations, $MgREE_2S_4$ compounds form. These compounds also show more structural types than analogous compounds in the Ca-REE-S system. Another difference from the REE-Ca-S system is that compounds like $MgREE_4S_7$ form, which indicates that the activities of the REE-sulfides in the two systems are somewhat different.

Solid solutions are absent in systems containing REE-sulfides and FeS (Flahaut, 1979). This is different than in the REE-(Ca or Mg)-S systems, where the heavy REE in particular show a wide range of solid solutions with CaS or MgS. However, some REE may dissolve in liquid 'FeS'. It is not clear if very low concentrations of REE sulfides remain in solid solution with 'FeS' when 'FeS' solidifies or if REE sulfides exsolve at low temperatures. The inhomogeneous distribution of Eu in 'FeS' from experiments spiked with Eu at the percent level (see above) and the phase diagram (Fig. 3) indicate that EuS is soluble in liquid FeS but not in solid FeS. This is similar to the apparent insolubility of CaS in solid FeS.

The phase equilibrium studies and the thermodynamic stability of the sequisulfides indicate that the assumptions of REE sesquisulfide and EuS formation during the experiments are reasonable. The partition coefficient of a lanthanide between sulfide and silicate according to Eq. (8b) is calculated from:

$$D \bullet c_f = \frac{a^{sulf.}_{MS_{1.5}}}{a^{sil.}_{MO_{1.5}}} = \frac{X^{sulf.}_{MS_{1.5}}}{X^{sil.}_{MO_{1.5}}} \frac{\chi^{sulf.}_{MS_{1.5}}}{\chi^{sil.}_{MO_{1.5}}} = \left(\frac{fS_2}{fO_2}\right)^{0.75} K \qquad \text{Eq. (10)}$$

In Eq. (10), a_i stands for the activity of species i and X_i for the mole fraction of $MS_{1.5}$ or $MO_{1.5}$ dissolved in sulfide or silicate, respectively. If we assume ideal solution behavior, Eq. (10) becomes:

$$D \bullet c_f = \frac{X^{sulf.}_{MS_{1.5}}}{X^{sil.}_{MO_{1.5}}} = \left(\frac{fS_2}{fO_2}\right)^{0.75} K \qquad \text{Eq. (11)}$$

The assumption of ideality or the assumption that the ratio of activity coefficients $\gamma MO_{1.5}/\gamma MS_{1.5}$ is about one was made because no data on REE sulfide activities in CaS are available. The phase diagram studies indicate that ideal solid solution may only apply to the EuS-CaS system. Effects due to deviations from ideality are discussed below. The equilibrium constant (K) in Eqs. (10) and (11) is calculated for each REE from the equilibrium constants for the formation of the sulfides ($K(M_2S_3)$) and oxides ($K(M_2O_3)$) from the constituent elements in their reference states as:

$$K = \left(\frac{K(M_2S_3)}{K(M_2O_3)}\right)^{0.5} \qquad \text{Eq. (12)}$$

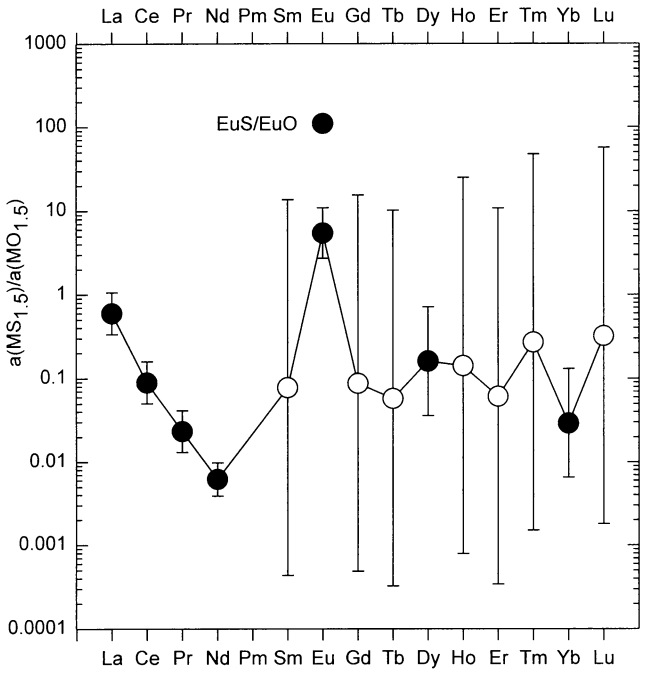

FIG. 5. Calculated sesquisulfide/sesquioxide activity ratios for the REE at 1200 °C (1473 K) for log $fO_2 = -15$ and log $fS_2 = -5.8$. For Eu, the respective monosulfide/sesquioxide and monosulfide/monoxide activity ratios are shown. Open symbols indicate ratios calculated from estimated thermodynamic data, while closed symbols are for ratios where experimentally determined thermodynamic data for the sulfides are available. The error bars result from uncertainties in the heat of formation of the REE sulfides. Assuming ideal solution of the REE in sulfides and oxides, the activity ratios equal mole fraction ratios, which in turn are proportional to sulfide/silicate partition coefficients. See text for data sources and details.

Similar expressions for the partition coefficient can be written for Eq. (8a) and equilibria involving EuO and EuS. The sources of the thermodynamic data for the REE-oxides and monosulfides are listed in Lodders and Fegley (1993), and data for the sesquisulfides were taken from Mills (1974) and Gmelin (1983) and references therein.

As shown in Eqs. (10) and (11), the mole fraction ratio $X(MS_{1.5})/X(MO_{1.5})$ equals the partition coefficient D times a conversion factor (c_f) from weight fractions to mole fractions. We are interested in the distribution of the REE at constant fO_2 and fS_2 conditions applicable to aubrites. Casanova (1990) estimated the fO_2 in aubrites as a function of temperature and Si content in the metal. At 1200 °C, mole fractions of Si in aubritic metals range from $<5 \cdot 10^{-5}$ to 10^{-2} indicating log fO_2 from >–15 to –17.5. Therefore, log $fO_2 = -15$ and –17.5 are chosen in the following calculations. The equilibrium value of log $fS_2 = -5.8$ above metal saturated FeS liquids at 1200 °C (Schürmann and Henke, 1972) is used for the S fugacity.

The sulfide/silicate activity ratios ($a(MS_{1.5})/a(MO_{1.5})$) for log $fO_2 = -15$ and log $fS_2 = -5.8$ at 1200 °C (1473 K) are shown in Fig. 5. The respective activity ratios for EuS/EuO and $EuS/EuO_{1.5}$ are plotted for Eu. In the case of ideal solution, these activity ratios should equal the mole fraction ratio in Eq. (11). The error bars result from the errors in the thermodynamic data for the heat of formation ($\Delta H_{f,298}$) of the REE sulfides. The open symbols are ratios calculated with estimated $\Delta H_{f,298}$ values for the sulfides, and the filled symbols are for ratios calculated with experimentally measured $\Delta H_{f,298}$ data. The estimated $\Delta H_{f,298}$ values are from Mills (1974) who lists uncertainties of ±130 kJ/mol for these enthalpy of forma-

tion values. In cases where $\Delta H_{f,298}$ data were subsequently measured experimentally, Mills' estimated enthalpy values agreed within ±5 kJ/mol, and the error bars in Fig. 5 could be significantly smaller than shown.

The predicted REE activity ratios in Fig. 5 are of the same order of magnitude (ranging from ~0.01 to ~1) as the experimentally determined partition coefficients. For the light REE, where the thermodynamic data are from experimental measurements, decreasing partition coefficients from La to Nd are predicted. This partitioning behavior is found for REE FeS_{liq}/$silicate_{liq}$ (Fig. 1). For the case of CaS_{sol}/$silicate_{liq}$ partition coefficients (Fig. 4), no data for Ce, Nd, or Pr were measured, and the trend from La to Sm is not indicative of whether the light REE follow the predicted trend. However, the opposite trend of D increasing, instead of D decreasing as predicted, is observed for (Ca,Mg)S_{liq}/$silicate_{liq}$ partition coefficients measured by Dickinson *et al.* (1991). This may indicate that activity coefficients of the REE in (Ca,Mg)S melts are not ideal. For the heavy REE, the predicted partitioning trend is less well determined due to the large uncertainties in the thermodynamic data. Therefore, we refrain from predicting any trend in heavy REE partitioning until better thermodynamic data for the heavy REE sulfides become available.

It is expected that Eu partitions more strongly into the sulfide than the neighboring Sm or Gd, or even La, Ce, Pr, or Nd, for which experimentally determined thermodynamic data exist. The predicted partition coefficient EuS/$EuO_{1.5}$ for trivalent Eu in the silicate is ~5.5 (assuming ideal solution and that the activity ratio equals the partition coefficient). A partition coefficient EuS/EuO of ~110 is calculated for divalent Eu in the silicate. Sulfides coexisting with silicates containing either Eu^{2+} or Eu^{3+} are expected to take up more Eu than Sm or Gd. In this respect, it is interesting to note that the fO_2 defined by the EuO/$EuO_{1.5}$ equilibrium is ~4 log units below the Fe-wüstite buffer. This is very close to the fO_2 of 3–6 log units below IW which is appropriate for aubrite formation. The EuS/EuO equilibrium is probably more important than the EuS/$EuO_{1.5}$ equilibrium, and larger partition coefficients are expected for Eu than for Sm and Gd. An overall decrease of the O fugacity from log fO_2 = –15 to –17.5 increases all partition coefficients because sulfides become more stable. For most REE equilibria ($MS_{1.5}$/$MO_{1.5}$) and the EuS/EuO equilibrium, the activity ratios shown in Fig. 5 increase by about a factor of 75 when the fO_2 is lowered by 2.5 log units while the EuS/$EuO_{1.5}$ activity ratio only increases by a factor of ~20.

These predictions for REE partition coefficients assume ideal solid solution of the REE sulfides in CaS or FeS and REE oxides in silicate. It seems that the REE 'FeS'/silicate partition coefficients most closely resemble the trend of predicted partition coefficients for the light REE and Eu, where the most certain predictions can be made. Small concentrations of REE sesquisulfides and EuS could dissolve in liquid FeS relatively ideally, but it may take *in situ* methods actually to determine the phase relations and activity data for the REE sulfides in liquid FeS because the liquid phase may not be quenchable at all.

Rare-earth-elements partition coefficients between solid CaS and liquid silicate increase from LREE to HREE, which is opposite to the predicted partition coefficients assuming ideal solid solution. This indicates a systematic decrease of the activity coefficients (γ) from LREE to HREE, so that in Eq. (10) the (predicted) activity equals the product of mole fraction (measured) and activity coefficient ($a = X \cdot \gamma$). This would be consistent with the observation that the range of solid solubility increases from light to heavy REE in the REE-Ca-S system. The same solution behavior for the REE (except Eu) is found for the REE-Mg-S system. Thus REE (Ca,Mg)S/silicate partition coefficients should show a similar trend as CaS/silicate partition coefficients. The well-established solid solubility of EuS in CaS indicates that ideal solid solution is probably a good assumption in this system. However, EuS and MgS are apparently insoluble (Van Tien and Khodadad 1970), and EuS solubility in (Ca,Mg)S is probably nonideal and limited. The activity coefficient of EuS in (Ca,Mg)S is expected to be much bigger than that in 'pure' CaS, meaning that partition coefficients for (Ca,Mg)S/silicate are smaller than those for CaS/silicate. Thus, the difference in Eu partitioning between CaS/silicate in this study and (Ca,Mg)S/silicate in the studies by Dickinson *et al.* (1990a,b, 1991) is most likely due to the differences in sulfide composition.

APPLICATION TO ENSTATITE ACHONDRITES

As mentioned in the introduction, it is necessary to know the REE distribution in the constituent minerals of aubrites and the REE partitioning data for the minerals of interest before any modeling of the origin of the phase assemblages in aubrites can be done. The REE in aubrites are mainly concentrated in CaS, with diopside and plagioclase being less important host phases. Olivine, enstatite, and troilite generally show very low abundances of the REE (for individual REE patterns in aubritic minerals, see Graham and Henderson, 1985; Floss and Crozaz, 1993; Lodders *et al.*, 1993; Wheelock *et al.*, 1994). It is important to note that 10 different types of REE patterns have been reported for oldhamite in the Bishopville, Bustee, Khor Temiki and Mayo Belwa aubrites, and at least three different patterns have been reported for diopside (Floss and Crozaz, 1993). The small number of available oldhamite analyses from the Norton County and Pena Blanca Spring aubrites are of one type, displaying negative Eu-anomalies (Lodders *et al.*, 1993; Wheelock *et al.*, 1994).

In the next sections, observations and possible aubrite formation scenarios that may or may not explain the REE distributions for aubrites are discussed. These are co-crystallization, fractional crystallization, and non-equilibrium melting. The discussion of co-crystallization leads to the long-standing question of whether oldhamite is formed by magmatic crystallization processes or if oldhamite in aubrites is a more or less altered refractory relict from an enstatite-chondrite-like precursor.

Wheelock (1990) and Wheelock *et al.* (1994) proposed that oldhamite in an oldhamite-dominated clast in the Norton County aubrite was formed by igneous processes from immiscible sulfide melts. Since most of the arguments for an igneous origin of oldhamite in aubrites come from their study, this is discussed in the section "Fractional crystallization?". In the section "Non-equilibrium melting", the observations by Wheelock *et al.* are integrated into the model of Lodders and Palme (1990). This model proposes that oldhamites in aubrites are refractory relicts from the enstatite-chondrite-like precursor and underwent different degrees of alteration, of which formation of an apparent 'igneous' clast is an extreme case.

Co-crystallization?

The first step to test if the mineral phases are in equilibrium and thus formed by crystallization from a single parental melt is to compare the REE concentration ratios in the aubritic mineral phases with the respective ratios of partition coefficients obtained at temperatures between 1200–1450 °C. These temperatures are typical of

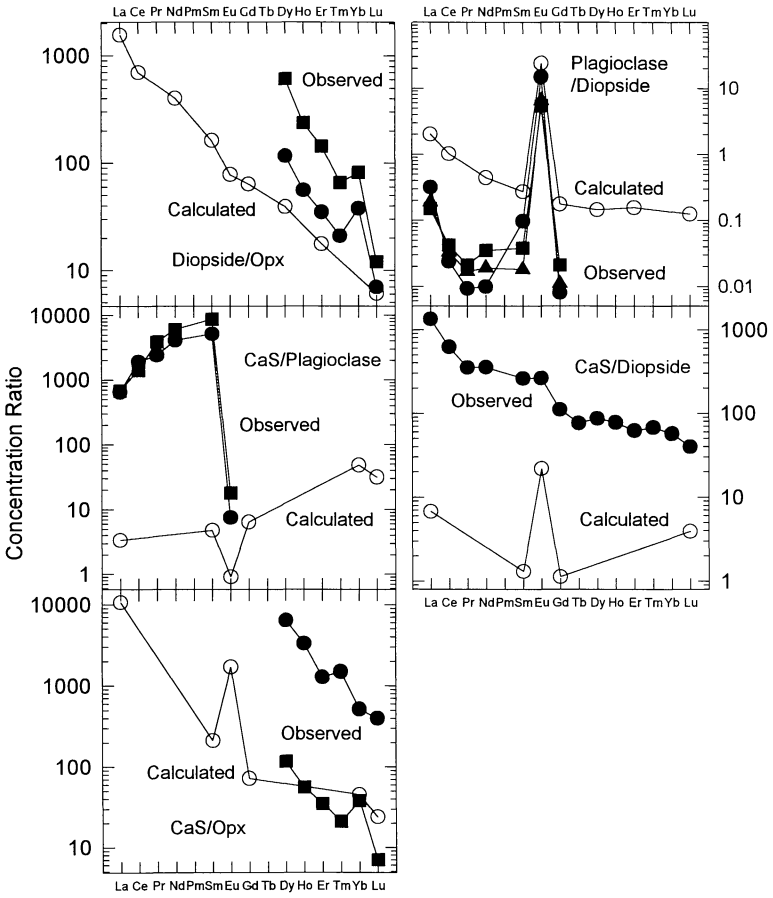

FIG. 6. Observed (closed symbols) and calculated (open symbols) concentration ratios for aubritic mineral pairs. Although the patterns qualitatively follow the trends expected from igneous partitioning, good matches are not obtained. In particular, the observed CaS/mineral ratios are 10–1000 times larger than predicted by igneous partitioning. See text for data sources.

magmatic differentiation processes. The comparison is shown in Fig. 6 for the pairs: diopside/enstatite, plagioclase/diopside, oldhamite/plagioclase, oldhamite/diopside, and oldhamite/enstatite. The REE mineral/melt partition coefficients used for plotting the calculated ratios in Fig. 6 are from Grutzeck *et al.* (1974; diopside), Drake and Weill (1975; plagioclase), Kennedy *et al.* (1993; pyroxene, olivine), and from Table 5 for oldhamite. Data for REE concentrations in individual aubritic minerals are from Graham and Henderson (1985), Floss *et al.* (1990), Floss and Crozaz (1993), and Wheelock *et al.* (1994). If possible, data to calculate ratios for mineral pairs were taken from analyses of minerals within an individual aubrite. Unfortunately, the light REE abundances in enstatite are below detection limits so that a comparison is possible only for the HREE. Likewise, the HREE in plagioclase are below detection limits, and a comparison is possible only for the LREE. Despite these limitations, the disparity of observed and predicted ratios indicates that the REE-bearing minerals are not in equilibrium and co-crystallization from a parent melt is very unlikely. This conclusion was also reached by Graham and Henderson (1985), who studied the REE distribution among the silicates in the Mayo Belwa aubrite by INAA.

Predicted and observed REE concentration ratios for diopside/opx differ by up to a factor of 10. Because REE abundances are extremely low in enstatite, the higher observed values indicate that diopside must have gained REE while not equilibrating with enstatite. Likewise, the predicted and observed values for the plagioclase/diopside pair also disagree by up to about a factor of 10, except for Eu, where predicted values are 2–4 times higher than observed ones. Although diopside often displays a REE pattern with negative Eu anomalies, relatively flat REE patterns are also observed (Floss and Crozaz, 1993) and are inconsistent with either enstatite/diopside or plagioclase/diopside equilibration. Observed CaS/plagioclase concentration ratios are up to ~1000 times higher than expected for La to Sm and indicate no equilibration. For Eu, the observed values are ~10 times larger than the predicted partitioning values. However, the overall partitioning trend of increasing CaS/plagioclase concentration ratios from LREE to HREE and Eu depletion suggests that some REE exchange took place.

Origin of Oldhamite in Aubrites

The discussion in the previous section shows that co-crystallization of oldhamite and other minerals is unlikely. Before other crystallization processes are discussed, it is necessary to address the question of where oldhamite in aubrites comes from. The similar oxidation states of aubrites and enstatite chondrites suggests that the aubrite parent body was assembled from material compositionally similar to enstatite chondrites. Watters and Prinz (1979) suggested that the precursor was similar to EL chondrites because addition of ~10% EL-chondritic plagioclase to aubrites yields good agreement with the composition of the bulk EL-chondrite silicates. Here we assume that EH-chondrites were similar to the precursor of aubrites because of the similar albite compositions in the two groups (Fogel *et al.*, 1988). Abundances of siderophile and chalcophile elements in aubrites also indicate that metal and sulfide abundances in the precursor were closer to those in EH-chondrites than in those EL chondrites (see Lodders *et al.*, 1993).

Most of the Ca in EH chondrites is present as CaS, and the amount of diopside and the amount of anorthite in plagioclase are small. In EH chondrites, the REE are mainly located in oldhamite (Lundberg and Crozaz, 1995). Condensation of REE into oldhamite in a reduced solar nebula gas can account for both the high REE abundances and for the diversity of REE patterns (Lodders and Fegley, 1993). Thus, the precursor supplies oldhamite which has high REE abundances and displays a variety of REE patterns.

Another potential source of oldhamite in aubrites is that Ca-bearing silicates (or melts) in the precursor material react to form CaS during heating of the aubrite parent body. The 'magmatic' origin of oldhamite was put forward by Dickinson and coworkers (1990a,b, 1991, 1996) because *in situ* formation of oldhamite was observed in their experiments and those by Jones and Boynton (1983). However, this process requires the sulfurization of diopside, anorthite or 'CaO' from a melt and probably did not occur on the APB because it requires the reduction of 'CaO' and a supply of S (*e.g.*, Larimer and Ganapathy, 1987; Lodders and Fegley, 1993). The *in situ* formation of oldhamite in the experiments by Jones and Boynton (1983) and Dickinson and coworkers (1990a,b, 1991, 1996) only occurred because the Mg or Al in their charges forced CaS formation (see Eqs. 6a,b). However, there is no reason to

believe that metallic Mg or Al are present on the aubrite parent body. Thus *in situ* formation of oldhamite on the APB is very unlikely.

Since the EH-chondrite-like precursor material already contains oldhamite, there is no need to postulate the formation of oldhamite from a silicate magma. However, very recently Fogel *et al.* (1996) showed that oldhamite may dissolve during melting of EH-chondritic material. Melting of the Indarch (EH) chondrite led to apparent CaS solution in the silicate in two out of the four experiments reported. Fogel *et al.* (1996) found that oldhamite was completely dissolved in silicate melt at 1400 °C. Dissolution of CaS in this experiment may be an artifact due to the extremely reducing conditions imposed by the Ta-O getter, which also led to the incorporation of >19 wt% Si in the Fe-metal. More oxidizing conditions, leading to ~0.5 wt% Si in metal, typical for aubrites (Casanova, 1990), will probably lead to less oldhamite solubility in silicate melts. Nevertheless, if this dissolution of CaS into silicate melts were important during differentiation of the APB, then there is the need to recrystallize oldhamite, since it is observed in aubrites. The petrologic observations in aubrites (see below) also suggest that oldhamite was present at temperatures even higher than those for which Fogel *et al.* found complete dissolution of CaS, which argues against this process. Clearly more experimental work is needed to decipher the potential importance of oldhamite dissolution in silicate melts, especially as a function of O fugacity. For the following discussion, it is assumed that oldhamite is always present during accretion and differentiation of the APB and that solid CaS coexists with silicate melt.

Fractional Crystallization of Silicates in Presence of Oldhamite?

Fractional crystallization and subsequent removal of crystallized phases from the melt is another potential crystallization process which was suggested for aubrites by Watters and Prinz (1979) and Okada *et al.* (1988) to explain the observed mineralogy of the Norton County aubrite. The crystallization sequence in simplified form is forsterite (first), enstatite, diopside, and plagioclase (last). Invoking the late crystallization of plagioclase to explain the REE distributions in Mayo Belwa is also consistent with the conclusions of Graham and Henderson (1985). If the REE are used for modeling aubrite petrogenesis, the presence of oldhamite must be considered. Since the major fraction of aubrites consists of enstatite, fractional crystallization requires high temperatures to produce an aubritic melt. The next two sections describe how oldhamite could behave during high temperature melting and subsequent fractional crystallization.

Petrologic Indicators of Fractional Crystallization–Based on petrological observations, Wheelock (1990) and Wheelock *et al.* (1994) proposed that oldhamite in an oldhamite-dominated clast in the Norton County aubrite formed by igneous processes from immiscible sulfide melts and that its REE abundances resulted from equilibration with the aubritic melt. These authors emphasize that they limit their discussion and arguments to the particular lithology in Norton County. This lithology is probably not representative of most oldhamite in aubrites but is certainly a good example to investigate the involvement of oldhamite in possible fractional crystallization processes in aubrites.

The major argument in favor of oldhamite crystallization from a melt is the large (up to 2 cm) crystal size of oldhamite, which cannot have formed by condensation processes. Two other observations that led Wheelock *et al.* (1994) to conclude that liquid oldhamite was present are: (1) the presence of forsterite grains that are (partially) surrounded by oldhamite, which was apparently molten while forsterite was already crystallized, and (2) the occurrence of rounded sulfide blebs in oldhamite, indicating the presence of two immiscible sulfide melts.

The question of how to melt aubritic oldhamite is long standing and controversial. Pure liquid CaS can almost certainly be ruled out because it is doubtful that temperatures reached the melting point of pure CaS (2450 °C) on the aubrite parent body. Temperatures as high as 2450 °C would have led to extensive vaporization of all rock-forming elements with the possible exceptions of Ca, Al, and Ti (Fegley and Cameron, 1987). Lodders *et al.* (1993) considered the melting point depression of aubritic CaS due to dissolved MnS, FeS, or MgS and calculated that Pena Blanca Spring oldhamite, containing up to 2 wt% total of Fe, Mn, and Mg, melts at ~2350 °C. Higher concentrations of other sulfides are necessary to suppress the melting point further, as the CaS-FeS phase diagram (Fig. 3) shows. In this system, an eutectic occurs at 1100 °C for 88 wt% FeS. However, the phase assemblage described by Wheelock *et al.* (1994) only contains ~4 wt% FeS and does not have the eutectic composition.

In addition to troilite, Wheelock *et al.* (1994) report ~10 vol% (~15 wt%) ferroan alabandite inclusions for this oldhamite. The ferroan alabandite occurs either as small, euhedral exsolution crystals or as rounded blebs in the oldhamite. Wheelock *et al.* (1994) proposed that "two mutually immiscible sulfide liquids—a Ca sulfide and a Mg-Fe-Mn-Cr-Na sulfide—formed in the silicate magma" to explain the occurrence of the alabandite blebs. However, another sulfide such as MnS must be dissolved in oldhamite to give the necessary melting point depression. The lowest liquidus temperature in the CaS-MnS system is at 1500 °C for ~77 wt% MnS (Leung and van Vlack, 1979), but the Norton County oldhamite contains much less MnS. Assuming that the system Mn(Fe)S-CaS is not too different from the MnS-CaS binary system, the solidus for the aubritic oldhamite containing ~19 wt% ferroan alabandite and troilite would be at ~1700 °C. This is below the melting point of forsterite and would explain the assemblage of oldhamite surrounding forsterite. At lower temperatures, CaS and MnS form a continuous series of solid solutions down to 1150 °C, where exsolution occurs (Skinner and Luce, 1971; Leung and van Vlack, 1979). Wheelock *et al.'s* (1994) observations of alabandite blebs in oldhamite plausibly indicate very rapid cooling of oldhamite. As a result, alabandite 'quenched out' as blebs before cooling slowed down to allow additional exsolution of euhedral crystals. Therefore, the occurrence of these blebs does not necessarily reflect the presence of two immiscible sulfides at high temperatures.

The amount of alabandite present in the particular oldhamite described by Wheelock *et al.* (1994) seems to be sufficient to allow formation of a liquid CaS-bearing melt. Note, however, that in most aubritic oldhamites smaller amounts of other sulfides are present leading to smaller melting point depressions. So these oldhamites were never molten.

If temperatures on the APB indeed reached 1700 °C or higher, oldhamite coexisted with a silicate melt from which enstatite starts crystallizing at 1580 °C. In almost all cases, the oldhamite was solid and not molten. Upon further cooling, diopside is expected to crystallize next, depending on how much CaO is present in the melt. Diopside was not reported for the particular clast studied by Wheelock *et al.* (1994), but aubrites typically contain ~ 1-3 vol% diopside (Watters and Prinz, 1979). Plagioclase crystallizes as a late phase (*e.g.*, Graham and Henderson, 1985; Okada *et al.*, 1988) as indicated

by its occurrence as smaller grains between forsterite and enstatite or as rim around sulfides (Wheelock *et al.*, 1994). If present, silica behaves like plagioclase. This fractional crystallization sequence seems to explain most of the textural observations for the particular clast investigated by Wheelock *et al.* (1994) and also several other aubritic lithologies described by Okada *et al.* (1988).

Rare-earth-elements Distribution during Fractional Crystallization–First we need to address how the REE were originally incorporated into the (undifferentiated) aubrite parent body (APB) and how a silicate melt could gain REE. The second step is to model how fractional crystallization redistributed the REE into various minerals and compare this to the observed REE abundance patterns in aubritic minerals.

The aubrite-EH-chondrite 'connection' described above indicates that the APB had a chondritic REE inventory and that initially the REE were concentrated at ~100 times chondritic levels in oldhamite supplied by the precursor. During fractional crystallization, temperatures above the melting point of enstatite would lead to large scale melting of the APB. In that case, all oldhamite present (whether melted because of solid solution formation with other sulfides or not) would equilibrate with the melt, as shown in all partitioning experiments. This would homogenize all the different REE patterns in oldhamite and lead to removal of the REE from the oldhamite into the melt. Assuming that 80% of the silicates were molten and that ~1% of oldhamite was present, the low CaS/silicate partition coefficients of ≤ 1 indicate that equilibration would reduce the REE abundances in oldhamite to $\sim \leq$ 1 times chondritic from the original ~100 times chondritic abundances. Thus oldhamite in equilibrium with a melt at high temperatures would be REE poor. Partition coefficients of about 100–200 are required to account for the high REE abundances observed in aubritic oldhamite. One could argue that the experimentally determined partition coefficients are too small because equilibrium was not reached between the CaS and silicate melt. However, this argument is contradicted by the partitioning experiments done with REE-bearing CaS as a reactant. These experiments gave D values within a factor of 2–4 of the D values obtained from experiments with REE-doped silicate. Furthermore, the independent work by Jones and Boynton (1983) and Dickinson *et al.* (1990a,b; 1991) also gave partition coefficients <<100.

A more efficient way to incorporate the REE into oldhamite by fractional crystallization is equilibration of oldhamite with an REE-enriched melt. Once enstatite crystallizes, the remaining silicate melt becomes enriched in REE because enstatite/melt and olivine/melt partition coefficients are small, and essentially none of the REE are removed from the melt into enstatite or olivine. The remaining REE-enriched melt of albitic-silica composition would then continue to equilibrate with the oldhamite, and the final REE abundances would be determined by the equilibrium of coexisting oldhamite and plagioclase. This crystallization sequence predicts only one type of REE pattern displaying a negative Eu-anomaly in all aubritic oldhamites. This type of REE pattern was found for oldhamite in the oldhamite-dominated clast in Norton County (Wheelock *et al.*, 1994) and for an oldhamite grain in igneous contact with plagioclase from Khor Temiki (Floss and Crozaz, 1993). However, the observed absolute abundances of REE in these oldhamites are much higher than expected from this crystallization process. The predicted CaS/plagioclase concentration ratios are a factor of 10 lower for Eu and about a factor of 1000 lower for the light REE than those observed (see also Fig. 6).

Problems with Crystallization Scenarios–Although fractional crystallization appears to be an attractive explanation of the mineralogy and textures in the oldhamite-dominated clast of the Norton County aubrite, it predicts REE abundances in oldhamite that are far too low. Furthermore, this clast is not representative of most oldhamites in aubrites. Fractional crystallization cannot explain the high REE abundances and different overall patterns observed in most aubritic oldhamites. There are also other problems with fractional crystallization.

First, Wheelock *et al.* (1994) report that in some cases forsterite contains plagioclase and sulfide inclusions. However, this is inconsistent with the above crystallization sequence of forsterite (first), enstatite, and plagioclase (last). Second, the scenario where oldhamite gains REE from a REE-rich melt after enstatite has precipitated fails to explain cases where REE-rich oldhamite enclosed in enstatite or pyroxenite was observed (Floss *et al.*, 1990; Kurat *et al.*, 1992). Third, fractional crystallization predicts only one type of REE pattern in oldhamite and cannot explain the variety of REE patterns for most of the oldhamite in aubrites. Fourth, fractional crystallization cannot account for the high REE abundances in oldhamite. Fifth, the high temperatures required for large scale melting of the APB (1700 °C or higher required to form oldhamite-alabandite liquids or 1580 °C required for melting of enstatite) would lead to substantial vaporization of Na, K, Si, and Mg (Fegley and Cameron, 1987). Complete loss of Na and K during heating of enstatite chondrites was observed at even lower temperatures of 1250–1400 °C (Fogel *et al.*, 1996). However, evaporative losses and, by implication, such high temperatures are ruled out because aubrites still contain significant abundances of Na and K and other volatile elements (*e.g.*, Biswas *et al.*, 1980; Wolf *et al.*, 1983; Lodders *et al.*, 1993). Last, Thiemens *et al.* (1994) report S-isotopic anomalies for oldhamite in the Norton County aubrite. Any large scale melting and equilibration of oldhamite with silicate melt would homogenize the S-isotopes and prevent preservation of anomalies. Homogenization would be even more pronounced if oldhamite had dissolved in the silicate.

Non-equilibrium Melting: A Preferred Differentiation Model of the Aubrite Parent Body

The problems described above for crystallization scenarios involving equilibration of oldhamite indicate that another process may be responsible for the variety of oldhamite occurrences and the diversity of REE abundance patterns observed in oldhamite and other aubritic minerals. As discussed earlier, it is unlikely that oldhamite formed *in situ* by sulfurization of the silicate minerals or melts. The more likely possibility is that oldhamite was inherited from the enstatite-chondrite-like precursor by the APB. Based on the results of their initial CaS/silicate partitioning experiments, Lodders and Palme (1990) originally proposed that oldhamite in aubrites is a relict condensate from the solar nebula. Later, the diversity of REE patterns in aubritic oldhamite was also used to suggest a relict origin for aubritic oldhamite (Floss *et al.*, 1990; Floss and Crozaz, 1993). The mass independent S isotopic anomalies observed by Thiemens *et al.* (1994) in Norton County oldhamite also indicate it is a relict nebula condensate.

The following scenario which involves non-equilibrium melting and subsolidus exchange reactions plausibly explains the observed phase assemblages and REE distribution in oldhamite and silicates in aubrites (Lodders *et al.*, 1993).

The aubrite parent body assembles from material compositionally similar to EH-chondrites, and heating and differentiation of

the APB occurs. The depletion of siderophile and chalcophile elements suggests that ~6 wt% FeS and 25 wt% metal segregate and form a core (Casanova *et al.*, 1993; Lodders *et al.*, 1993). However, aubrites still contain some minor metal and troilite, and segregation of metal and sulfide into the core was not complete. This indicates that melting at high temperatures, which would allow efficient metal and sulfide segregation from a silicate melt, was not a large scale event. While the minimum temperatures required for eutectic Fe-FeS segregation are ~1000 °C, temperatures must increase to the melting point of enstatite (1580 °C) to allow most of the silicate to become liquid. A mechanism that would heat almost the entire APB is difficult to envision. The other points described at the end of the last section also argue against large scale melting.

Segregation of troilite and metal during core formation could cause oldhamite removal into the core. The FeS-CaS phase diagram (Fig. 3) shows that an FeS-CaS eutectic melt can form at 1100 °C, and Vogel and Heumann (1941) state that the ternary Fe-FeS-CaS eutectic seems to fall at the same temperature. However, significant removal of oldhamite can be excluded because it is still present in aubrites. A more quantitative indicator of possible oldhamite loss is the oldhamite/silicate ratio in enstatite chondrites and aubrites (a normalization of the modal content of oldhamite to silicate is used to take the presence of larger amounts of sulfide and metal in E-chondrites into account). The oldhamite/silicate ratios in enstatite chondrites range ~0.003–0.015 by weight (Keil, 1968). Similar ratios of ~0.003 are found in aubrites (Khor Temiki, Pena Blanca Spring) where oldhamite abundances have been determined (Hey and Easton, 1967; Lodders *et al.*, 1993). Thus, CaS removal into the APB core was apparently not an efficient process. Iron sulfide and CaS must be intimately mixed to produce the eutectic, but most oldhamite occurs as isolated grains in silicates. The Fe-FeS melt has a higher density (~4.6 g/cm^3) than CaS (2.5 g/cm^3), and gravitational forces can remove the Fe-FeS melt before any mixing with CaS occurs. Furthermore, associations of oldhamite and troilite showing eutectic textures, as described by Vogel and Heumann (1941), have not been reported in aubrites.

Another indicator that significant amounts of troilite were not mixed with oldhamite are the low REE abundances in troilite. These are near or below detection limits in ion probe measurements (*e.g.*, Wheelock *et al.*, 1994). Oldhamite contains high abundances of the REE, and REE partitioning between troilite and oldhamite would have led to higher REE concentrations in troilite (~1–10 times chondritic), as indicated by the FeS and CaS partition coefficients. Thus, the segregating FeS cannot take up any significant amounts of REE, and FeS segregation probably did not influence the bulk silicate REE pattern in aubrites. The similarity of aubritic oldhamite REE patterns to those in oldhamites of unequilibrated enstatite chondrites also shows that most of the aubritic oldhamite did not equilibrate with other minerals during core formation event(s).

Melting cannot have been a large scale process but may have been restricted to local events. Shock melting by impacts on the APB leading to short non-equilibrium melting episodes seems to be a plausible heat source. Depending on how efficient shock melting was, oldhamite and its REE pattern will be more or less altered. Most oldhamite in aubrites is small and comparable in grain size to that observed in enstatite chondrites (30–200 μm; Larimer and Ganapathy, 1987), but larger grains of millimeter size up to extreme cases of 2 cm (Wheelock *et al.*, 1994) are also occasionally observed. The larger oldhamite grains could be produced by sintering.

Once silicates start melting, small CaS grains can float and accumulate because of the lower density of CaS (2.5 g/cm^3) compared to that of silicates (~3–3.3 g/cm^3). The collection of CaS by a silicate melt may be the reason for the CaS-rich, 1.6 cm long impact-produced melt vein in the Jajh deh Kot Lalu (EL6)-enstatite chondrite (Rubin *et al.*, 1995). Sintering of larger accumulations of CaS can lead to larger CaS aggregates. Sintering in presence of a melt is a very fast process (of a few hours) and can easily lead to larger grains (Kingery *et al.*, 1976). Sintering of CaS grains was also observed in the partitioning experiments where rounded CaS grains or grain surfaces connected to other grains were present. During sintering, the REE can move from the oldhamite into the surrounding melt, but sintering timescales may be shorter than the time needed for REE equilibration. Further experiments are needed to investigate this.

The first melt generated in aubrites is of albitic-silica-rich composition (Fogel, 1994). It is questionable if an albitic melt preferentially incorporates Eu, as solid plagioclase does. However, fast melting and cooling could lead to oldhamite sintering in such a melt. If plagioclase forms upon cooling, the REE, and in particular Eu, may move from oldhamite into plagioclase until exchange becomes frozen. This would explain why larger oldhamites, which are associated with plagioclase, have high REE abundances and a REE pattern with a negative Eu-anomaly. Generally, solid-liquid exchange or solid-solid exchange, as may also occur during thermal metamorphism, are most effective on small grains. Still, the observed oldhamite/plagioclase REE ratios are generally far from equilibrium (Fig. 6), and the Sm/Eu ratio in plagioclase is also about a factor of 10–100 away from that expected from plagioclase/melt partition coefficients of Sm and Eu.

An extreme case is shock melting and the production of large amounts of silicate liquid at high temperatures. This can make the collection process of oldhamite grains more efficient and also bring oldhamite into contact with other sulfides, which were not extracted into the core. Depending on the peak temperatures reached and on the absolute amounts of oldhamite and other sulfides present, melting of oldhamite may occur to produce oldhamite-forsterite assemblages as observed by Wheelock *et al.* (1994). However, while accumulation, sintering, and subsequent melting of oldhamite can occur rapidly, the timescales for heating and cooling were apparently not sufficient for equilibrium REE redistribution from oldhamite into other phases. Some of the following observations also show that oldhamite was involved in exchange reactions to different degrees. In all these cases, REE are distributed from oldhamite into other phases, which is plausible if we accept that REE-rich oldhamite was inherited by the APB.

Oldhamite inclusions in enstatite and diopside are reported in some cases (Floss and Crozaz, 1993). If diopside is formed solely by crystallization from a melt, only the REE pattern expected from diopside/melt partitioning should be observed, but different types of patterns are reported by Floss and Crozaz (1993). Lodders *et al.* (1993) proposed that the different REE patterns in diopside can be understood if diopside was formed from oldhamite. If oldhamite reacts with enstatite to form diopside and forsterite, as suggested by Fogel *et al.* (1988), the diopside would inherit the REE inventory of the oldhamite.

The observation by Wheelock *et al.* (1994) of plagioclase with an anorthite-rich rim and albite-rich interior also indicates that an oldhamite-plagioclase exchange reaction took place. This reaction could have occurred at subsolidus temperatures during thermal

metamorphism. Crystallization cannot explain the observed reversed zoning in plagioclase. Instead, crystallization predicts an anorthite-rich interior and albitic rim. Any exchange process should also lead to zoned REE profiles in minerals coexisting with CaS. Further REE measurements on such mineral assemblages may reveal that the REE underwent metamorphic redistribution. Preliminary ion probe investigations of an enstatite-oldhamite assemblage from the Pena Blanca Spring aubrite (Fahey *et al.,* 1995) show a falling concentration gradient of the REE from the oldhamite-enstatite interface towards the enstatite interior. More investigations of major element (Ca, Mg, Mn, Fe) distributions in oldhamite and coexisting minerals may also provide additional information about the extent of (metamorphic) exchange reactions. More primitive oldhamite should display higher Fe and Mg but lower Mn concentrations than metamorphically altered oldhamite (Larimer and Ganapathy, 1987; Lodders *et al.*, 1993).

It seems that most of the oldhamite inherited from the enstatite chondrite-like precursor may never have come in contact with melt or exchanged REE with other minerals. The high REE abundances and variety of REE patterns for most oldhamites in aubrites are still strikingly close to those in unequilibrated enstatite chondrites. Still, more investigations of major element and REE distributions among coexisting minerals in aubrites as well as experimental studies of mineral phase relations are needed to test the model proposed above and to obtain a better understanding about the evolution of the aubrite parent body.

Acknowledgments–Experimental work on REE partitioning was performed as part of my doctoral thesis at the Max-Planck Institut für Chemie, Mainz, Germany. I thank H. Palme for discussions and the staff of the TRIGA Mark-II reactor of the Johannes Gutenberg-Universität Mainz for technical support. Experiments on the CaS/silicate system were performed at the Lunar and Planetary Laboratory in Tucson, Arizona, during a three months stay in 1990. I appreciate the hospitality and helpful comments by M. J. Drake. I also thank W. Bilodeau (Tucson) for assistance performing the XRD analysis. Many helpful discussions and suggestions by B. Fegley helped to improve the manuscript. Thoughtful reviews by B. Fogel, H. Newsom, and A. Rubin are appreciated. The data analysis and preparation of this paper were supported by NASA grant NAGW-2861.

Editorial handling: K. Keil

REFERENCES

BISWAS S., WALSH T., BART G. AND LIPSCHUTZ M. E. (1980) Thermal metamorphism of primitive meteorites–XI. The enstatite meteorites: Origin and evolution of a parent body. *Geochim. Cosmochim. Acta* **44,** 2097–2110.

CASANOVA I. (1990) Geochemistry of metal segregation in aubrites and the origin of their metallic phases. Ph. D. thesis, University of New Mexico. 97 pp.

CASANOVA I., KEIL K. AND NEWSOM H. E. (1993) Composition of metal in aubrites: Constraints on core formation. *Geochim. Cosmochim. Acta* **57,** 675–682.

DICKINSON T. L. AND MCCOY T. (1996) Experimental REE partitioning in oldhamite: Implications for the igneous origin of aubritic oldhamite (abstract). *Lunar Planet. Sci.* **27,** 309–310.

DICKINSON T. L., LOFGREN G. E. AND MCKAY G. A. (1990a) REE partitioning between silicate liquid and immiscible sulfide liquid: The origin of the negative Eu anomaly in aubrite sulfides (abstract). *Lunar Planet. Sci.* **21,** 284–285 .

DICKINSON T. L., LOFGREN G. E. AND MCKAY G. A. (1990b) Sulfide fractionation and the origin of the negative Eu anomaly in aubrites (abstract). *Meteoritics* **25,** 358.

DICKINSON T. L., LOFGREN G. E. AND MCKAY G. A. (1990c) REE partitioning between silicate liquid and immiscible sulfide liquid: The origin of aubritic sulfides (abstract). *EOS Trans. AGU* **71,** 1434.

DICKINSON T. L., LOFGREN G. E. AND MCKAY G. A. (1991) On the magmatic origin of oldhamite in aubrites (abstract). *Lunar Planet. Sci.* **22,** 319–320.

DRAKE M. J. AND WEILL D. F. (1972) New rare earth element standards for electron microprobe analysis. *Chem. Geol.* **10,** 179–181.

DRAKE M. J. AND WEILL D. F. (1975) Partition of Sr, Ba, Ca, Y, Eu^{2+}, Eu^{3+}, and other REE between plagioclase feldspar and magmatic liquid: An experimental study. *Geochim. Cosmochim. Acta* **39,** 689–712.

ELISEEV A. A. AND KUZMICHYEVA G. M. (1990) Phase equilibrium and crystal chemistry in rare earth ternary systems with chalcogenide elements. In *Handbook on the Physics and Chemistry of Rare Earth*, vol. 13 (eds. K. A. Gschneidner and L. Eyring), pp. 191–281. Elsevier North-Holland, New York, New York.

FAHEY A., HUSS G., WASSERBURG G. J. AND LODDERS K. (1995) REE abundances and Cr isotopic composition of oldhamite and associated minerals from the Pena Blanca Spring aubrite (abstract). *Lunar Planet. Sci.* **26,** 385–386.

FEGLEY B. AND CAMERON A. G. W. (1987) A vaporization model for iron/silicate fractionation in the Mercury protoplanet. *Earth Planet. Sci. Lett.* **82,** 207–222.

FLAHAUT J. (1979) Sulfides, selenides and tellurides. In *Handbook on the Physics and Chemistry of the Rare Earth*, vol. 4 (eds. K. A. Gschneidner and L. Eyring), pp. 1–87. Elsevier North-Holland, New York, New York.

FLAHAUT J., DOMAGE L. AND PATRIE M. (1961) Combinaisons formées par les sulfures des éléments du groupe des terres rares. II. – Le diagramme d'équilibre du système sulfure d'yttrium-sulfure de calcium. *Bull. Soc. Chim. Fr.* 105–108.

FLAHAUT J., DOMAGE L. AND PATRIE M. (1963) Combinaisons formées par les sulfures des éléments du groupe des terres rares. VI. – Étude cristallographique des phases ayant le type structural du phosphure de thorium Th_3P_4. *Bull. Soc. Chim. Fr.*, 2048–2054.

FLOSS C. AND CROZAZ G. (1993) Heterogeneous REE patterns in oldhamite from aubrites: Their nature and origin. *Geochim. Cosmochim. Acta* **57,** 4039–4057.

FLOSS C., STRAIT M. M. AND CROZAZ G. (1990) Rare earth elements and the petrogenesis of aubrites. *Geochim. Cosmochim. Acta* **54,** 3553–3558.

FOGEL R. A. (1994) Aubrite basalt vitrophyres: High sulfur silicate melts and a snapshot of aubrite formation (abstract). *Meteoritics* **29,** 466–467.

FOGEL R. A., HESS P. C. AND RUTHERFORD M. J. (1988) The enstatite chondrite-achondrite link (abstract). *Lunar Planet Sci.* **19,** 342–343.

FOGEL R. A., WEISBERG M. K. AND PRINZ M. (1996) The solubility of CaS in aubrite silicate melts (abstract). *Lunar Planet. Sci.* **27,** 371–372.

GMELIN HANDBUCH DER ANORGANISCHEN CHEMIE. (1983) ed. H. Bergmann. 8th ed. Springer Verlag, Berlin, Germany. 607 pp.

GRAHAM A. L. AND HENDERSON P. (1985) Rare earth element abundances in separated phases of Mayo Belwa, an enstatite achondrite. *Meteoritics* **20,** 141–149.

GRUTZECK M., KRIDELBAUGH S. AND WEILL D. (1974) The distribution of Sr and REE between diopside and silicate liquid. *Geophys. Res. Lett.* **1,** 273–275.

HEUMANN T. (1942) Die Löslichkeit von Eisensulfid in Kalziumsulfid bei der eutektischen Temperatur. *Archiv Eisenhüttenw.* **15,** 557–558.

HEY M. H. AND EASTON A. J. (1967) The Khor Temiki meteorite. *Geochim. Cosmochim. Acta* **31,** 1789–1792.

JANAF THERMOCHEMICAL TABLES (1985) eds. M. W. Chase *et al.*, *J. Phys. Chem. Ref. Data* **14,** Suppl. No 1.

JONES J. H. AND BOYNTON W. V. (1983) Experimental geochemistry in very reducing systems: Extreme REE fractionation by immiscible sulfide liquids (abstract). *Lunar Planet. Sci.* **14,** 353–354.

KEIL K. (1968) Mineralogical and chemical relationships among enstatite chondrites. *J. Geophys. Res.* **73,** 6945–6976.

KENNEDY A. K., LOFGREN G. E. AND WASSERBURG G. J. (1993) An experimental study of trace element partitioning between olivine, orthopyroxene and melt in chondrules: Equilibrium values and kinetic effects. *Earth Planet. Sci. Lett.* **115,** 177–195.

KINGERY W. D., BOWEN H. K. AND UHLMAN D. R. (1976) *Introduction to Ceramics.* John Wiley & Sons, New York, New York. 1032 pp.

KUBASCHEWSKI O. (1982) *Iron-Binary Phase Diagrams.* Springer Verlag, Berlin, Germany. 125–128 pp.

KUBASCHEWSKI O. AND ALCOCK C. B. (1979) *Metallurgical Thermochemistry.* Pergamon, New York, New York. 183 pp.

KURAT G., ZINNER E. AND BRANDSTÄTTER F. (1992) An ion microprobe study of an unique oldhamite-pyroxenite fragment from the Bustee aubrite (abstract). *Meteoritics* **27,** 246–247.

LARIMER J. W. AND GANAPATHY R. (1987) The trace element chemistry of CaS in enstatite chondrites and some applications regarding its origin. *Earth Planet. Sci. Lett.* **15,** 123–134.

LEUNG C.-H. AND VAN VLACK L. H. (1979). Solubility limits in binary (Ca,Mn) chalcogenides. *J. Amer. Ceram. Soc.* **62,** 613–616.

LODDERS K. (1991) Spurenelementverteilung zwischen Sulfid und Silikatschmelze und kosmochemische Anwendungen. Ph. D. thesis, Univ. Mainz. 176 pp.

LODDERS K. (1995) Experimental partitioning of rare earth elements between sulfides (FeS,CaS) and silicate melt and applications to enstatite achondrites (abstract). *Symp. Antarc. Meteor.* **20,** 140–144.

LODDERS K. (1996) Oldhamite in enstatite achondrites (aubrites). *Proc. NIPR Symp. Antarct. Meteor.* **9th,** 127–142.

LODDERS K. AND FEGLEY B. (1993) Lanthanide and actinide chemistry at high C/O ratios in the solar nebula. *Earth Planet. Sci. Lett.* **117,** 125–145.

LODDERS K. AND PALME H. (1989) Europium anomaly produced by sulfide separation and implications for the formation of enstatite achondrites (aubrites) (abstract). *Meteoritics* **24,** 293–294.

LODDERS K. AND PALME H. (1990) Fractionation of REE during aubrite formation: The influence of FeS and CaS (abstract). *Lunar Planet. Sci.* **21,** 710–711.

LODDERS K. AND PALME H. (1991) On the chalcophile character of molybdenum: Determination of sulfide/silicate partition coefficients of Mo and W. *Earth Planet. Sci. Lett.* **103,** 311–324.

LODDERS K., PALME H. AND DRAKE M. J. (1990) The origin of oldhamite in enstatite achondrites (aubrites) (abstract). *EOS Trans. AGU* **71,** 1434.

LODDERS K., PALME H. AND WLOTZKA F. (1993) Trace elements in mineral separates of the Pena Blanca Spring aubrite: Implications for the evolution of the aubrite parent body. *Meteoritics* **28,** 538–551.

LUNDBERG L. L. AND CROZAZ G. (1995) The origin of oldhamite in unequilibrated enstatite chondrites. *Geochim. Cosmochim. Acta* **59,** 3817–3831.

MASUDA M. (1967) Lanthanides in the Norton County achondrite. *Geochem. J.* **2,** 111–135.

MEDVEDEV V. A., BERMAN G. A., GURVICH L. V., YUNGMAN V. S., VOROBIEV A. F. AND KOLESOV V. OP. (1979) *Termicheskie Konstanty Veshchastv (Thermal Constants of Substances), Be, Mg, Ca, Sr, Ba, Ra* (ed. V. P. Glusko) Part IX, Akad. Nauk USSR, Viniti, Moscow, USSR. 522 pp.

MEYER A. AND PINK H. (1973) A partial phase diagram for the system EuS-FeS. *J. Less. Comm. Metals* **30,** 314–316.

MILLS K. C. (1974) *Thermodynamic Data for Inorganic Sulphides, Selenides and Tellurides.* Butterworths, London, U.K. 845 pp.

NEWSOM H. E. AND DRAKE M. J. (1983) Experimental investigation of the partitioning of phosphorous between metal and silicate phases: Implications for the Earth, Moon and eucrite parent body. *Geochim. Cosmochim. Acta* **47,** 93–100.

OKADA A., KEIL K., TAYLOR G. J. AND NEWSOM H. (1988) Igneous history of the aubrite parent asteroid: Evidence from the Norton County enstatite achondrite. *Meteoritics* **23,** 59–74.

RUBIN A. E., SCOTT E. R. D. AND KEIL K. (1995) Shock metamorphism of enstatite chondrites (abstract). *Lunar Planet. Sci.* **26,** 1197–1198.

SCHMITT R. A, SMITH R. H., LACH J. E., MOSEN A. W., OLEHEY D. A. AND VASILEVSKIS J. (1963) Abundances of the fourteen rare-earth elements, scandium, and yttrium in meteoritic and terrestrial matter. *Geochim. Cosmochim. Acta* **27,** 577–622.

SCHMITT W., PALME H. AND WÄNKE H. (1989) Experimental determination of metal/silicate partition coefficients for P, Co, Ni, Cu, Ga, Ge, Mo, and W and some implications for the early evolution of the Earth. *Geochim. Cosmochim. Acta* **53,** 173–185.

SCHÜRMANN E. AND HENKE H. J. (1972) Zur Thermodynamik des Systems Eisen-Schwefel. *Giessereiforsch.* **24,** 1–9.

SKINNER B. J. AND LUCE F. D. (1971) Solid solutions of the type (Ca, Mg, Mn, Fe)S and their use as geothermometer for the enstatite chondrites. *Amer. Mineral.* **56,** 1269–1296.

STOFKO M., SCHMIEDL J. AND ROSENQVIST T. (1974) Thermodynamics of iron-sulfur oxygen melts at 1200 °C. *Scan. J. Metall.* **3,** 113–118.

THIEMENS M. H., BREARLEY A., JACKSON T. AND BOBIAS G. (1994) Detection of a ^{35}S excess in an oldhamite separate from Norton County (abstract). *Meteoritics* **29,** 540–541.

TSAI H. L. AND MESCHTER P. J. (1981) Phase relationships in CaS-rare earth sulfide systems. *J. Electrochem. Soc.* 128, 2229–2232.

TURKDOGAN E. T. (1983) *Physicochemical Properties of Molten Slags and Glasses.* The Metals Society, London, United Kingdom. 516 pp.

VAN TIEN V. AND KHODADAD P. (1970) Étude des combinaisons entre les sulfures SmS et EuS avec les sulfures MS (M=Mg, Ca, Sr, Ba); stabilité thermique de SmS. *Bull. Soc. Chim. Fr.* **8/9,** 2888–2890.

VOGEL R. AND HEUMANN T. (1941) Das System Eisen-Eisensulfid-Kalziumsulfid. *Archiv Eisenhüttenw.* **15,** 195–199.

WÄNKE H., KRUSE H. PALME H. AND SPETTEL B. (1977) Instrumental neutron activation analysis of lunar samples and the identification of primary matter in the lunar highlands. *J. Radioanal. Chem.* **38,** 363–378.

WASSON J. T. AND KALLEMEYN G. W. (1988) Compositions of chondrites. *Phil. Trans. Roy. Soc. Lond.* **A325,** 535–544.

WATTERS T. R. AND PRINZ M. (1979) Aubrites: Their origin and relationship to enstatite chondrites. *Proc. Lunar Planet. Sci. Conf.* **10th,** 1073–1093.

WHEELOCK M. M. (1990) The magmatic history of an aubrite parent asteroid: Evidence from igneous clasts and trace elements. MS Thesis, University. of New Mexico. 78 pp.

WHEELOCK M. M., KEIL K., FLOSS C. TAYLOR G. J. AND CROZAZ G. (1994) REE geochemistry of oldhamite-dominated clasts from the Norton County aubrite: Igneous origin of oldhamite. *Geochim. Cosmochim. Acta* **58,** 449–458.

WICKMAN H. W., ROBBINS M. AND BUEHLER E. (1970) Mössbauer isomer shifts of dilute Eu^{2+} ions. *Phys. Lett.* **31A,** 59–60.

WOLF R., EBIHARA M., RICHTER G. R. AND ANDERS E. (1983) Aubrites and diogenites: Trace element clues to their origin. *Geochim. Cosmochim. Acta* **47,** 2257–2270.